Gastroenterology 2020;158:2236–2249

Editing Myosin VB Gene to Create Porcine Model of Microvillus Inclusion Disease, With Microvillus-Lined Inclusions and Alterations in Sodium Transporters

Amy C. Engevik,[1,2] Alexander W. Coutts,[3] Izumi Kaji,[1,2] Paula Rodriguez,[3] Felipe Ongaratto,[3] Milena Saqui-Salces,[4] Ramya Lekha Medida,[4] Anne R. Meyer,[1,2] Elena Kolobova,[1,2] Melinda A. Engevik,[5] Janice A. Williams,[1,2] Mitchell D. Shub,[6] Daniel F. Carlson,[3] Tamene Melkamu,[3] and James R. Goldenring[1,2,7,8]

[1]Department of Surgery, Vanderbilt University School of Medicine, Nashville, Tennessee; [2]The Epithelial Biology Center, Vanderbilt University School of Medicine, Nashville, Tennessee; [3]Recombinetics Inc, Saint Paul, Minnesota; [4]Department of Animal Science, University of Minnesota, Saint Paul, Minnesota; [5]Baylor College of Medicine and Texas Children's Hospital, Houston, Texas; [6]Phoenix Children's Hospital and University of Arizona College of Medicine-Phoenix, Phoenix, Arizona; [7]Cell and Developmental Biology, Vanderbilt University School of Medicine, Nashville, Tennessee; and [8]Nashville Veterans Affairs Medical Center, Nashville, Tennessee

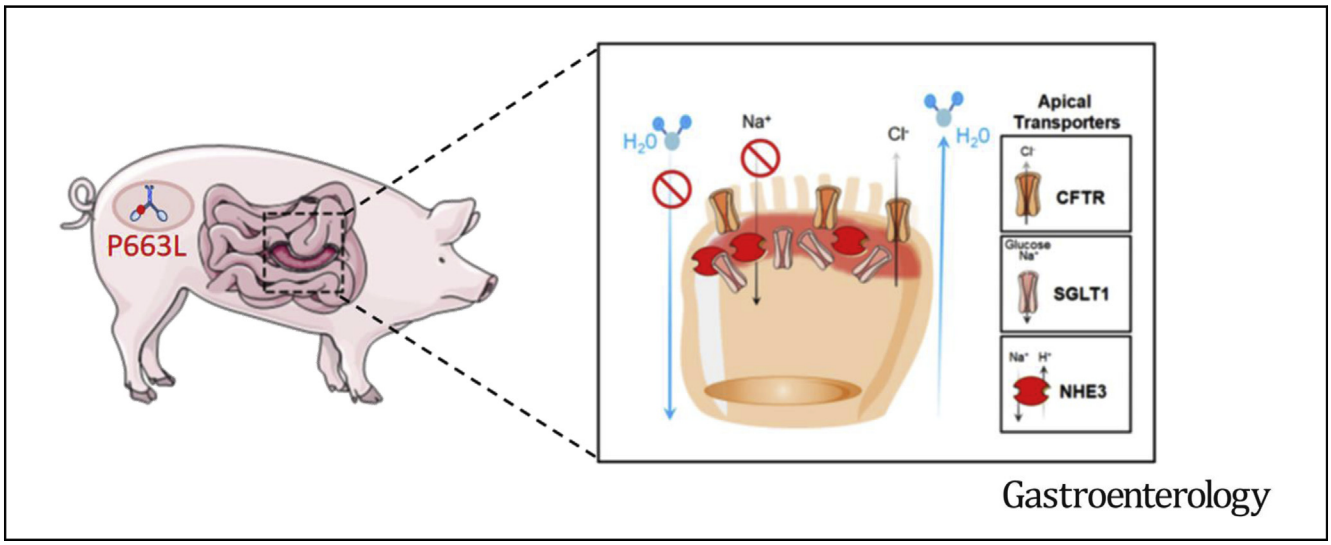

BACKGROUND & AIMS: Microvillus inclusion disease (MVID) is caused by inactivating mutations in the myosin VB gene (*MYO5B*). MVID is a complex disorder characterized by chronic, watery, life-threatening diarrhea that usually begins in the first hours to days of life. We developed a large animal model of MVID to better understand its pathophysiology. **METHODS:** Pigs were cloned by transfer of chromatin from swine primary fetal fibroblasts, which were edited with TALENs and single-strand oligonucleotide to introduce a P663–L663 substitution in the endogenous swine *MYO5B* (corresponding to the P660L mutation in human MYO5B, associated with MVID) to fertilized oocytes. We analyzed duodenal tissues from patients with MVID (with the MYO5B P660L mutation) and without (controls), and from pigs using immunohistochemistry. Enteroids were generated from pigs with MYO5B(P663L) and without the substitution (control pigs). **RESULTS:** Duodenal tissues from patients with MVID lacked MYO5B at the base of the apical membrane of intestinal cells; instead MYO5B was intracellular. Intestinal tissues and derived enteroids from MYO5B(P663L) piglets had reduced apical levels and diffuse subapical levels of sodium hydrogen exchanger 3 and SGLT1, which regulate transport of sodium, glucose, and water, compared with tissues from control piglets. However, intestinal tissues and derived enteroids from MYO5B(P663L) piglets maintained CFTR on apical membranes, like tissues from control pigs. Liver tissues from MYO5B(P663L) piglets had alterations in bile salt export pump, a transporter that facilitates bile flow, which is normally expressed in the bile canaliculi in the liver. **CONCLUSIONS:** We developed a large animal model of MVID that has many features of the human disease. Studies of this model could provide information about the functions of MYO5B and MVID pathogenesis, and might lead to new treatments.

Keywords: Malabsorption; Missense Mutation; Motor Protein; Plasma Membrane.

Abbreviations used in this paper: **BSEP, bile salt export pump; CFTR, cystic fibrosis transmembrane conductance regulator; KO, knockout; MVID, microvillus inclusion disease; NHE3, sodium hydrogen exchanger 3; PCR, polymerase chain reaction; P-ERM, phosphorylated ezrin-radixin-moesin; RFLP, restriction fragment length polymorphism; TEM, transmission electron microscopy; TPN, total parenteral nutrition; WT, wild-type.**

Most current article

0016-5085/$36.00
https://doi.org/10.1053/j.gastro.2020.02.034

Microvillus inclusion disease (MVID) is a congenital diarrhea disorder that results from inactivating mutations in the molecular motor, Myosin Vb (MYO5B).[1–3] Among congenital diarrhea disorders, MVID is one of the most severe, with life-threatening diarrhea developing in the first week of life, requiring early management with administration of total parenteral nutrition (TPN).[4] No definitive treatments exist for MVID outside of chronic TPN or small bowel transplantation. In a subset of individuals, treatment is also accompanied by liver transplantation.[5,6] Whether TPN contributes to the liver cholestasis observed in individuals with MVID has been controversial.[7,8]

While the prevalence of MVID in the general population is low (fewer than 200 known cases, orpha.net), there is an increased incidence of MVID in Turkey and in the Navajo Nation in the American Southwest.[9] In the Navajo tribe, the majority of individuals with MVID have a missense mutation (1979C>T p.Pro660Leu, exon 16 referred to as MYO5B(P660L).[3,10] Before 2015, MVID studies relied solely on in vitro cell lines and human tissue.[2,11–13] Recently, mouse models have been generated to elucidate the pathogenesis of MVID by characterizing alterations in physiological function and intestinal structure resulting from loss of Myo5b in vivo.[14–17] While mouse models of human diseases are useful, complex diseases such as MVID may be better understood using large animal models that are closer to human physiology. To date, no large animal model has been generated for MVID. To better understand the pathogenesis of human MVID, we developed a porcine model of MVID using gene editing to express a mutation in MYO5B (P663L) homologous with the human MYO5B mutation found in the Navajo tribe (P660L). Piglets expressing the MYO5B(P663L) mutation demonstrated the presence of microvillus-lined inclusions, a hallmark of MVID, along the length of the small and large intestine. Alterations in sodium transporters (sodium hydrogen exchanger 3 [NHE3] and SGLT1) that facilitate enterocyte water absorption were present, with prominent subapical expression of these transporters in MYO5B(P663L) pig small and large intestine. The cystic fibrosis transmembrane conductance regulator (CFTR), which secretes chloride into the intestinal lumen, was maintained on the apical membrane of enterocytes in MYO5B(P663L) enterocytes. Immunostaining of wild-type (WT) and MYO5B(P663L) liver showed alterations in bile salt export pump (BSEP) at the apical canalicular membrane of hepatocytes in MYO5B(P663L) pigs compared to WT. These results show that villus blunting, as well as liver alterations that likely contribute to cholestasis, occurs early on in pigs with the Navajo mutation in MYO5B. Development of treatments that promote the proper delivery of sodium transporters to the apical membranes of enterocytes and BSEP to the canalicular membrane of hepatocytes may be efficacious in treating MVID.

WHAT YOU NEED TO KNOW

BACKGROUND AND CONTEXT

Microvillus inclusion disease (MVID) is caused by inactivating mutations in the myosin VB gene (*MYO5B*).

NEW FINDINGS

We used gene editing to develop a large animal model of MVID that has many features of the human disease.

LIMITATIONS

At the early postnatal stage analyzed in the MYO5B(P663L) piglets, the full spectrum of disease observed in patients with MVID may not be present.

IMPACT

Studies of this model could provide information about MVID pathogenesis and lead to development of treatments.

Methods

TALEN Design, Assembly, and RNA Synthesis

All TALENs were designed using the TAL Effector Nucleotide Targeter 2.0 software and assembled using standard methods.[18–23] Linearized TALEN DNA was transcribed in vitro using the mMessage Machine T3 kit (Ambion, Austin, TX). Synthesis reactions were assembled in a 20 μL reaction with 1 μg linearized plasmid DNA, 1× NTP/CAPs (Ambion), 1× reaction buffer (Ambion), and 2 μL enzyme mix (Ambion). Reactions were incubated for 2 hours at 37°C, treated with Turbo DNase (Invitrogen, Carlsbad, CA), then cleaned up with the RNeasy Mini Kit (Qiagen, Hilden, Germany).

Cell Culture and Transfection of Swine Embryonic Fibroblasts

Fetal fibroblasts isolated from day 38–45 Landraces pig fetuses were cultured in 1× high-glucose Dulbecco's modified Eagle medium (Invitrogen) with 10% fetal bovine serum (Atlas Biologicals, Fort Collins, CO), 2 mM L-glutamine (Corning, Corning, NY), 10 mM HEPES buffer (Lonza, Basel, Switzerland), 1× penicillin/streptomycin solution (Corning), 5 μg/mL Apo-Transferrin (Sigma, St Louis, MO), 20 ng/mL recombinant human IGF-1 (R&D Systems, Minneapolis, MN), and 25ng/mL recombinant human epidermal growth factor (R&D Systems) and transfected using the Neon Transfection System (Thermo Fisher Scientific, Waltham, MA). Briefly, each transfection reaction included 600,000 fibroblasts, 1 μg of TALEN RNA, and 0.2-nmol homology-directed repair oligonucleotide, and the transfection reaction was pulsed once at 1800 V for 20 milliseconds using the Neon transfection system (Thermo Fisher Scientific). Transfected cells were cultured 3 days at 30°C before splitting for restriction fragment length polymorphism (RFLP) analysis and plating for colony isolation at 38.5°C. Individual colonies were collected in 10-cm dishes, where 80–250 transfected cells were plated and allowed to grow for 10–14 days, and individual colonies were aspirated under gentle trypsinization. The picked colonies were subsequently genotyped by RFLP and sequence analysis.

Detection and Sequence Validation of Gene Modification

Transfected cells harvested at day 3 were prepared for polymerase chain reaction (PCR) analysis by pelleting and resuspending in PCR-safe lysis buffer (10 mm Tris·Cl [pH 8.0];

2 mM EDTA; 2.5% [vol/vol] Tween-20; 2.5% [vol/vol] Triton X-100; and 100 μg/mL proteinase K) at approximately 1000 cells/μL, followed by incubation at 55°C for 60 minutes and 95°C for 15 minutes. Typically, 1 μL of prepared lysate was used in a 2× AccuStart II PCR SuperMix (QuantaBio, Beverly, MA); all other applications were according to the manufacturer's protocol. Gene modification in individual colonies was detected by RFLP analysis and direct sequencing of PCR amplicons, characterized by TOPO cloning (Invitrogen) and sequencing.

Animal Husbandry and Cloning

MYO5B(P663L) pigs were produced under license of chromatin transfer technology from Hematech to Cooperative Resources International Center for Biotechnology (Verona, WI). All animal work was performed in Recombinetics Inc facilities under its Animal Welfare Assurance #A4728-01. All animal protocols were reviewed and approved by the Institutional Animal Care and Use Committee.

Three MYO5B(P663L) pigs were born alive via caesarean section. However, 1 MYO5B(P663L) pig died on delivery. The tissue harvested from this pig lacked well-developed epithelial tissues when examined by H&E and intestinal epithelial markers were poorly detected. Two MYO5B(P663L) pigs were euthanized within 24 hours of delivery by intracardiac barbiturate injection after standard procedures of the Veterinary Diagnostic Laboratory of the University of Minnesota under its Animal Welfare Assurance #A3456-01. Three WT pigs were age-matched from different litters and examined as controls. For all experiments, there were 2 MYO5B(P663L) pigs and 3 WT pigs.

Immunostaining

Paraffin. –Tissue was excised and immediately fixed in 4% paraformaldehyde or 10% neutral buffered formalin overnight at 4°C. Fixed tissue was embedded in paraffin and 6-μm sections were used for immunostaining. Slides were heated before deparaffinization. Antigen retrieval was performed using Target Retrieval Solution citrate buffer (pH 6) (cat. no. S1699; Dako, Glostrup, Denmark) using a pressure cooker set on high for 15 minutes. Slides were cooled in antigen retrieval on ice before blocking using protein block serum-free (cat. no. X0909; Dako) for 1.5 hours at room temperature. Primary antibodies were added to antibody diluent with background reducing components (cat. no. S3022; Dako) after the protein block and incubated overnight at 4°C. Sections were washed 3 times in 1× phosphate-buffered saline for 5 minutes per wash. Secondary antibodies were diluted 1:200 using antibody diluent (cat. no. S0809; Dako) and incubated for 1 hour in the dark at room temperature. Hoechst 33342 (cat. no. 62249, 10 mg/mL; Thermo Fisher Scientific) in phosphate-buffered saline was applied to slides for 5 minutes to stain the nuclei. Slides were washed 3 times in phosphate-buffered saline for 5 minutes each wash. Prolong Gold Antifade (cat. no. P36934; Thermo Fisher Scientific) was used to coverslip each slide. Slides were imaged using an Axio microscope or a LSM 880 with Airyscan (Zeiss, Oberkochen, Germany). Antibodies used are listed in Supplementary Table 1.

All authors had access to the study data and reviewed and approved the final manuscript.

Results

Generation of a Microvillus Inclusion Disease Pig Model by Gene Editing

To generate a pig model of MVID, we mimicked a missense mutation p.Pro660Leu in the *MYO5B* gene identified in the Navajo population.[3,10] *MYO5B*^{P660L} lies within exon 28 of the swine *MYO5B* gene at position 663, which shares 100% amino acid identity with human exon 16 (Supplementary Figure 1*A*). TALENs flanking *MYO5B*^{P663L} were designed and subsequently transfected into fetal Landrace fibroblasts with or without a homology-directed repair oligonucleotide containing the *P663L* mutation and a *Hin*dIII RFLP site (Supplementary Figure 1*B*). Cutting and homology repair efficiency of the TALENs was determined by Surveyor and RFLP assay, respectively (Supplementary Figure 1*C* and *D*). Colonies derived from single cells were isolated and genotyped for the *MYO5B*^{P663L} mutation (data not shown). Owing to the low efficiency of the genome engineering tools, no homozygous colonies were isolated besides 1 semi-homozygous clone (clone 44) that had the intended P663L mutation on 1 allele, and a 70-bp deletion on the other allele, which removes a portion of exon 28 and intron 27, including the predicted splice receptor (allele 1). The deletion on allele 1 is predicted to create a null mutation, as it leads to the incorporation of intron 27 and downstream stop codons. The semi-homozygous clone was subjected to chromatin transfer, resulting in 2 viable pregnancies and 4 F0 male piglets (Supplementary Figure 1*E*). *MYO5B*$^{P663L/KO}$, referred to as MYO5B(P663L), F0, and WT control pigs were genotyped by RFLP and sequence validated (Supplementary Figure 1*F* and *G*).

MYO5B(P663L) Pigs Display Intestinal Abnormalities Characteristic of Microvillus Inclusion Disease

The distribution of MYO5B in duodenal biopsy tissue from healthy individuals and Navajo patients with MVID (MYO5B[P660L]) was examined by immunostaining. In healthy control tissue, MYO5B appeared predominantly expressed at the base of the brush border. MVID patients with the MYO5B P660L mutation lacked MYO5B near the apical membrane, instead MYO5B was observed intracellularly (Supplementary Figure 2*A*). The altered localization of MYO5B in Navajo MVID patients is consistent with previous findings showing that the P660L mutation creates a rigor dysfunction in the motor, which can bind F-actin but cannot complete a motor stroke.[12]

Similar to healthy humans, the duodenum of WT pigs showed MYO5B primarily restricted to the base of the brush border as delineated by dipeptidyl peptidase 4 (DPPIV) staining. MYO5B(P663L) pigs showed MYO5B primarily expressed near the Golgi complex (GM130) with little expression at the base of the apical membrane (Supplementary Figure 2*B*). Measurement of mean

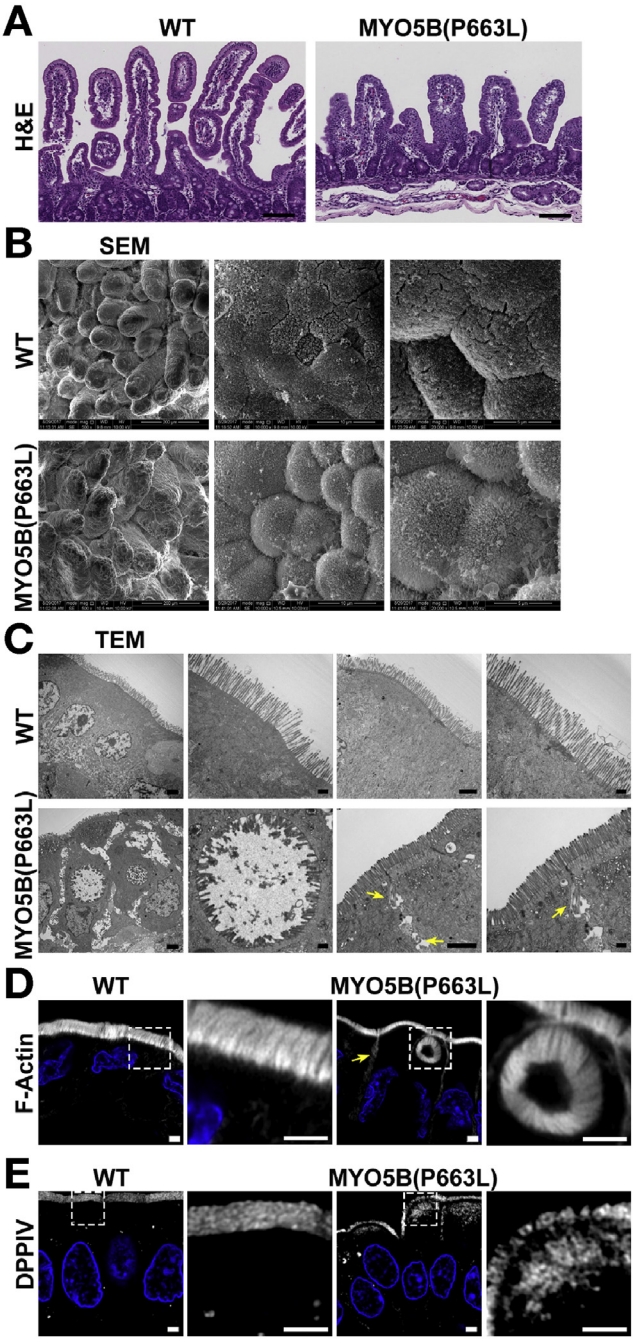

Figure 1. Changes in small intestinal cell morphology resulting from MYO5B(P663L) mutation. (*A*) H&E of WT and MYO5B(P663L) pig duodenum. Scale bars: 50 μm. (*B*) Scanning electron microscopy of pig small intestine demonstrating uniform villi in WT pigs. The cells along the villi of WT pig duodenum appeared well-aligned with uniform microvilli packing. MYO5B(P663L) pigs had broad, stunted villi with prominent cell rounding evident at the tips with disorganized microvilli packing. (*C*) TEM of the duodenum of neonatal WT and MYO5B(P663L) pigs demonstrated well-formed brush border in WT pig enterocytes. MYO5B(P663L) enterocytes had shortened microvilli, densely packed subapical vesicles, lateral microvilli in gaps between cells (indicated by *yellow arrows*) and the presence of intracellular microvillus-lined inclusions. (*D*) Prominent F-actin–positive inclusions were observed in the small intestine of MYO5B(P663L) pigs. No inclusions were observed in WT pigs. (*E*) Dipeptidyl peptidase 4 (DPPIV) immunostaining of WT pig duodenum showed apical localization, in contrast MYO5B(P663L) pig duodenum had diffuse subapical DPPIV Scale bars: 2 μm.

fluorescence intensity of MYO5B in WT and MYO5B(P663L) pigs demonstrated no difference, suggesting that protein levels are not significantly altered by the MYO5B(P663L) mutation, but that the MYO5B(P663L) mutation likely prevents proper function of MYO5B (Supplementary Figure 2*C*). The immunostaining of MYO5B in MYO5B(P663L) piglets resembled that of human MVID patients with the Navajo P660L mutation.[12]

H&E staining of the duodenum of WT and MYO5B(P663L) pigs showed large differences in villi size and structure, MYO5B(P663L) pigs exhibited stunted and thickened villi compared to WT (Figure 1*A*), consistent with reports demonstrating villus atrophy in patients with MVID.[24–26] Duodenal tissue of WT piglets showed well-structured villi and uniformed packing of microvilli (Figure 1*B*). MYO5B(P663L) duodenal tissue demonstrated profound cell rounding at the tips of villi and cells lacking organized microvilli reminiscent of findings reported by Cutz et al[27] that proximal intestinal enterocytes of MVID patients appeared rounded and smoothed, lacking well-developed microvilli.

Transmission electron microscopy (TEM) and F-actin staining confirmed changes in cellular morphology in MYO5B(P663L) piglet duodenal tissue, where large intracellular inclusions and lateral microvilli were observed that are characteristic of MVID[24,27] (Figure 1*C* and *D*). The presence of lateral microvilli in humans with MVID has not been fully recapitulated in mouse models of MVID.[28–30] MYO5B(P663L) pigs also exhibited a large accumulation of vesicles below the apical membrane that was not observed in WT pigs, consistent with data obtained from intestinal biopsies from MVID patients.[31]

Altered Expression of Apical Transporters in MYO5B(P663L) Pigs

The small intestine is the primary site of fluid and electrolyte absorption.[32] Loss of apical expression of transporters that promote water absorption and maintenance of chloride secretion through CFTR may be the primary cause of MVID-associated diarrhea.[14] SGLT1 is the primary transporter for absorption of galactose and glucose and is responsible for Na^+-dependent sugar transport, which is accompanied by water transport, thus facilitating hydration.[32] Immunostaining of the duodenum of WT pigs showed SGLT1 on the apical membrane of enterocytes (Figure 2*A*). In MYO5B(P663L) pigs, SGLT1 expression was reduced on the apical membrane and subapical SGLT1 was observed. Confocal high-magnification images revealed SGLT1 located below the brush border in MYO5B(P663L) pigs, consistent with data obtained from patients with MVID and Myo5b knockout (KO) mice.[12,14] NHE3 also promotes small intestinal Na^+ and water absorption. In patients with MVID and in Myo5b KO mouse models, NHE3 is mislocalized,

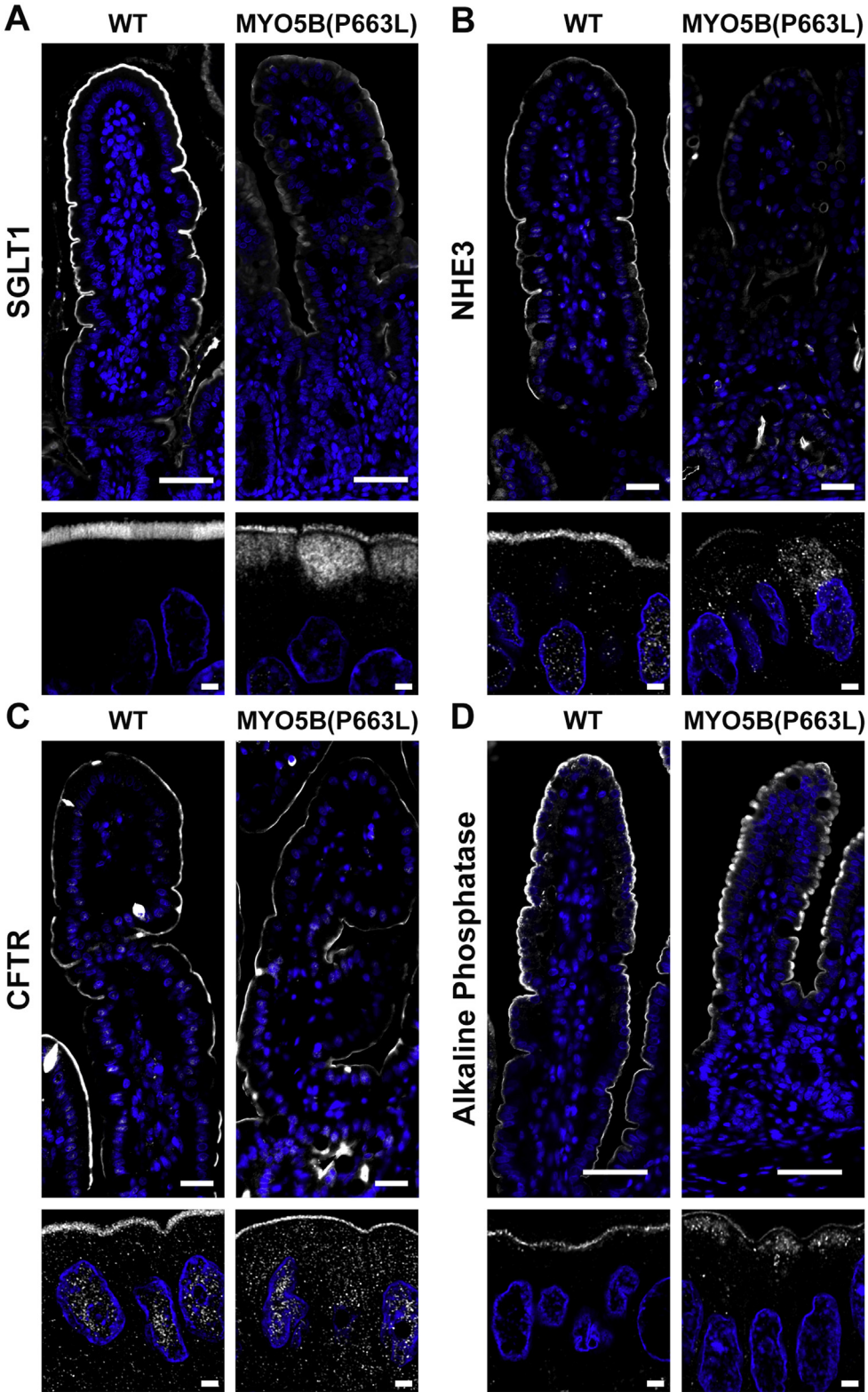

Figure 2. Localization of apical transporters in the duodenum of neonatal pigs. (*A*) Confocal imaging demonstrated the presence of diffuse SGLT1 below the apical brush border in MYO5B(P663L) enterocytes compared to WT. (*B*) NHE3 was observed below the apical membrane in MYO5B(P663L) enterocytes with reduced apical localization compared to WT. (*C*) CFTR was observed on the apical membrane of MYO5B(P663L) enterocytes as in WT. (*D*) Alkaline phosphatase immunostaining showed intracellular localization of alkaline phosphatase in MYO5B(P663L) pigs compared to WT. Scale bars: 50 μm and 2 μm in low and high magnification, respectively.

displaying predominantly intracellular expression.[14,17,31,33] In the duodenum of WT pigs, NHE3 expression was restricted to the brush border as expected (Figure 2*B*). In contrast, MYO5B(P663L) pigs exhibited NHE3 in inclusions and diffusely below the apical membrane in the duodenum.

CFTR is a chloride channel that is present on the apical membrane of enterocytes. CFTR is a target of cholera toxin

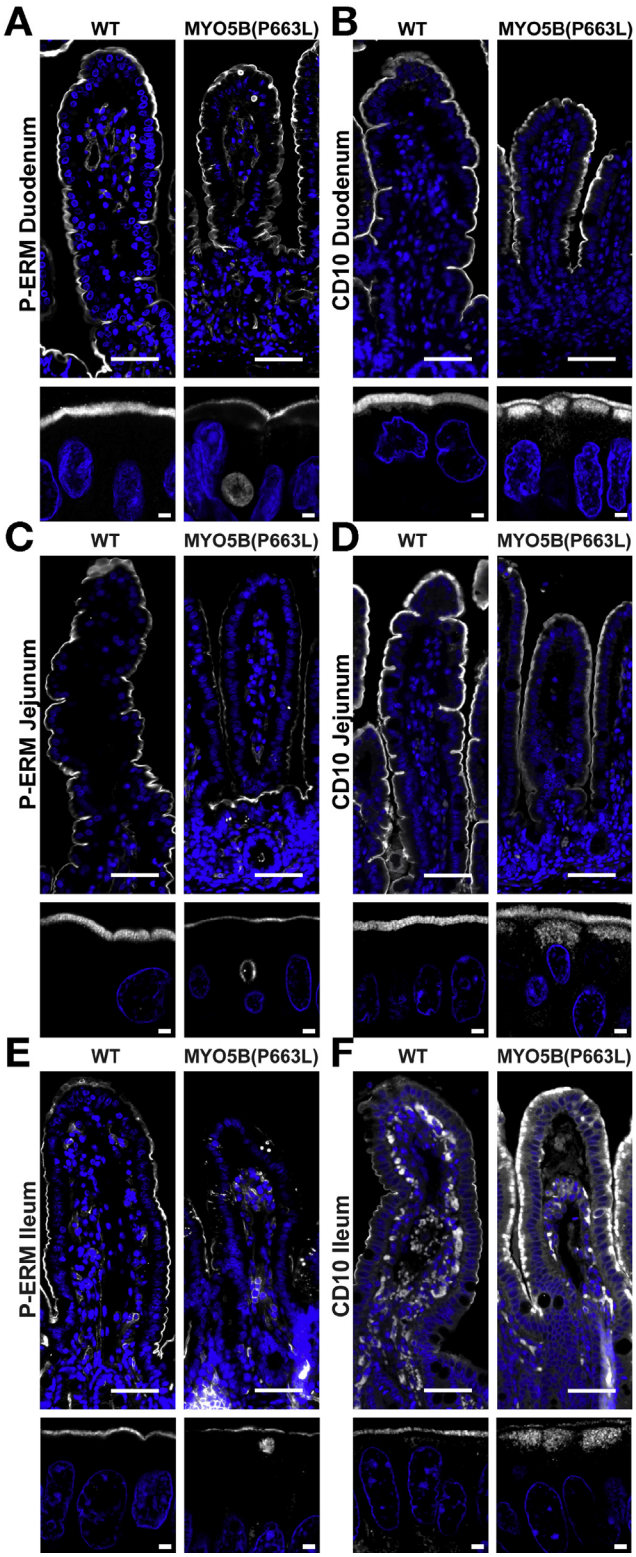

Figure 3. Alterations in brush border markers persist along the length of the small intestine in MYO5B(P663L) pigs. (*A*) P-ERM immunostaining showed normal apical localization in WT enterocytes. In contrast, MYO5B(P663L) enterocytes had prominent inclusions that were P-ERM–positive. P-ERM immunostaining also demonstrated decreased microvilli height in MYO5B(P663L) enterocytes compared to WT enterocytes. (*B*) CD10 has been used to diagnose MVID in patients. CD10 immunostaining had apical localization in WT enterocytes. In MYO5B(P663L) enterocytes, CD10 was observed diffusely below the apical membrane. (*C, E*) Immunofluorescence staining showed P-ERM positive inclusions throughout the jejunum and ileum in MYO5B(P663L) pigs. (*D, F*) CD10 localized subapically in MYO5B(P663L) enterocytes in the jejunum and ileum. Scale bars: 50 μm and 2 μm in low and high magnification, respectively.

resulting in profound secretory diarrhea by the active secretion of Cl^- into the gut lumen, which draws water by osmosis, resulting in diarrhea.[34,35] In the duodenum of WT pigs, CFTR was localized to the apical membrane of enterocytes (Figure 2*C*). In MYO5B(P663L) pigs, CFTR was largely maintained on the apical membrane, in contrast to the subapical expression of SGLT1 and NHE3 in MYO5B(P663L) enterocytes. The observed pattern of CFTR expression in MYO5B(P663L) pigs closely mirrored findings in Myo5b KO mouse models and in human MVID tissue.[14,33] The loss of apical Na^+ transporters and the retention of CFTR in the brush border of enterocytes in MYO5B(P663L) pigs suggests that the inability to absorb Na^+, coupled with functional Cl^- secretion, may be the primary source of MVID-associated diarrhea.

Intestinal alkaline phosphatase is mislocalized in enterocytes of patients with MVID and in Myo5b KO mouse models.[14,16,31] Consistent with previous studies, MYO5B(P663L) pigs exhibited decreased apical alkaline phosphatase and large amounts of cytoplasmic alkaline phosphatase compared to WT pigs by immunofluorescence. Collectively, these observations suggest that the pig model of MVID shares critical characteristics with human MVID disease and supports a central role for MYO5B in trafficking NHE3, SGLT1, and alkaline phosphatase to the apical membrane of enterocytes.

Intestinal Abnormalities Persist Throughout the Small and Large Intestines of MYO5B(P663L) Piglets

Due to the limited availability of tissue biopsies from MVID patients, the impact of mutations in MYO5B along the length of the small intestine is not clear. Data from mouse models indicate that the duodenum is most affected by altered expression of MYO5B compared to the jejunum and ileum.[17] Germline Myo5b KO mice exhibit the greatest number of inclusions in the duodenum, with fewer inclusions present in the jejunum and fewer still in the ileum. In addition to the decreasing number of inclusions along the length of the small intestine, structural abnormalities of fused villi occurred at a higher frequency in the duodenum compared to the jejunum and ileum of germline Myo5b KO mice.[17] However, in humans, it has been reported that major alterations exist along the entire small bowel in MVID patients.[36] WT pigs exhibited phosphorylated ezrin-radixin-moesin (P-ERM) expression on the apical membrane of enterocytes along the whole length of the small intestine. Inclusions positive for P-ERM were observed in the duodenum, jejunum, and ileum at similar frequency in

MYO5B(P663L) pigs (Figure 3*A*, *C*, and *E*). Subapical expression of CD10, a brush border membrane–associated peptidase, has been used to diagnose MVID.[36–38] Micrographs of CD10 immunostaining demonstrate that in WT pigs, CD10 is localized to the brush border of enterocytes throughout the small intestine (Figure 3*B*, *D*, and *F*). In MYO5B(P663L) pigs, subapical accumulation of CD10 was observed in the duodenum, jejunum, and ileum. NHE3 expression along the small intestine showed a similar pattern to CD10, with decreased expression of NHE3 in the brush border and large pools of subapical NHE3 in the jejunum and ileum of MYO5B(P663L) pigs compared to WT pigs (Supplementary Figure 3).

Immunostaining of the proximal and distal colon of WT pigs showed apical localization of NHE3 and SGLT1. In contrast, MYO5B(P663L) pigs exhibited large amounts of subapical NHE3 and decreased apical localization of SGLT1 in the proximal and distal colon (Supplementary Figure 4*A*–*D*). Moreover, large intracellular inclusions defined by gamma actin immunofluorescence were observed in the proximal and distal colon of MYO5B(P663L) pigs (Supplementary Figure 4*E*), which was surprising because no inclusions were previously reported in the colons of Myo5b KO mice.[17] Collectively, these data suggest that MYO5B(P663L) pigs have altered expression of apical membrane components along the entire length of the small and large intestines.

Enteroids Generated From MYO5B(P663L) Pigs Recapitulate In Vivo Findings

Enteroids were generated from WT and MYO5B(P663L) pigs to further elucidate enterocyte abnormalities resulting from mutation of MYO5B. Gross morphology of enteroids appeared similar between WT and MYO5B(P663L) enteroids (Figure 4*A*). However, immunostaining of enteroids showed a poorly developed brush border and mislocalized P-ERM in MYO5B(P663L) enteroids (Figure 4*A*). Additionally, MYO5B(P663L) enteroids had subapical inclusions consistent with in vivo findings (Figure 4*B*). To promote differentiation of enteroids, 3D enteroids were plated onto Transwells to form a 2D monolayer and were cultured using an air liquid interface (Figure 4*C*). WT enteroid monolayers demonstrated a well-defined brush border marked by F-actin and apical NHE3 expression (Figure 4*D*). In contrast MYO5B(P663L) enteroids displayed large amounts of intracellular NHE3 in enterocytes. SGLT1 immunofluorescence was localized to the apical membrane of WT enterocytes, while MYO5B(P663L) enterocytes showed cytoplasmic expression of SGLT1 (Figure 4*E*). We observed similar levels of CFTR on the apical membrane of WT and MYO5B(P663L) enterocytes, although subapical expression of CFTR was present in WT and MYOB(P663L) enteroid monolayers (Figure 5*A*).

To determine whether CFTR was functional in WT and MYO5B(P663L) enteroids, we used a forskolin swelling assay in 3D enteroids. Administration of forskolin increases the level of intracellular cyclic adenosine monophosphate resulting in activation of CFTR and swelling of enteroids.[39,40] Measurement of enteroids before and after forskolin-induced swelling demonstrated that MYO5B(P663L) enteroids swelled to a greater degree than WT enteroids, suggesting that CFTR is functional in MYO5B(P663L) enteroids and may have greater activity than WT enteroids (Figure 5*B* and *C*). The increased swelling of MYO5B(P663L) enteroids could also be attributed to the decreased water absorption that results from improper apical localization of NHE3 and SGLT1. We postulate that CFTR activation and the decreased ability of MYO5B(P663L) enteroids to absorb water both contribute to the increased swelling observed in these enteroids.

The intestines of the MYO5B(P663L) piglets showed no formed stool and remarkably clear fluid in the lumen throughout. Fecal chloride levels were measured to determine whether chloride secretion was higher in MYO5B(P663L) piglets compared to WT in vivo (Figure 5*D*). Chloride concentration was significantly higher in the fecal content of MYO5B(P663L) pigs compared to WT suggesting that CFTR-mediated chloride secretion was likely occurring in vivo and that MYO5B(P663L) pigs exhibited a chloride secretory diarrhea.

MYO5B(P663L) Pigs Exhibit Altered Expression of Apical Transporters in Hepatocytes

Studies have reported that many individuals with MVID manifest cholestasis and progressive liver disease.[41] Recent reports have also noted mutations in MYO5B that do not result in recurrent diarrhea (MVID) in humans, but are associated with low γ-glutamyltransferase cholestasis.[42,43] Previously, alterations in liver function in patients with MVID were attributed to prolonged use of TPN.[7,8] However, recent studies suggest that mutations in MYO5B are the direct cause of hepatocyte alterations that cause cholestasis.[41–43] Currently, no published data exist regarding alterations in liver after loss of Myo5b in animal models of MVID. H&E staining showed the presence of lipid droplets in hepatocytes from WT piglets, but no other gross alterations were observed in liver morphology (Figure 6*A*). Immunostaining for MYO5B in WT pig hepatocytes showed MYO5B closely associated with the canaliculi as defined by MRP2 immunostaining. In MYO5B(P663L) pig hepatocytes, MYO5B appeared in clusters farther away from the canaliculi and had decreased cytoplasmic expression of MYO5B compared to WT hepatocytes (Figure 6*B* and *C*). ABCB1 (MDR1) is normally expressed in the canaliculi of hepatocytes and is responsible for the secretion of xenobiotics across the bile canaliculi membrane.[44] MYO5B(P663L) pig hepatocytes showed decreased expression of ABCB1 at the apical membrane and more diffuse expression at the apical membrane compared to WT hepatocytes (Figure 6*D*).

To determine whether the pig MYO5B(P663L) mutation resulted in liver alterations of other canalicular membrane proteins, we immunostained liver sections for the BSEP. Previous investigations have noted a disrupted canalicular distribution of BSEP in patients with mutations in

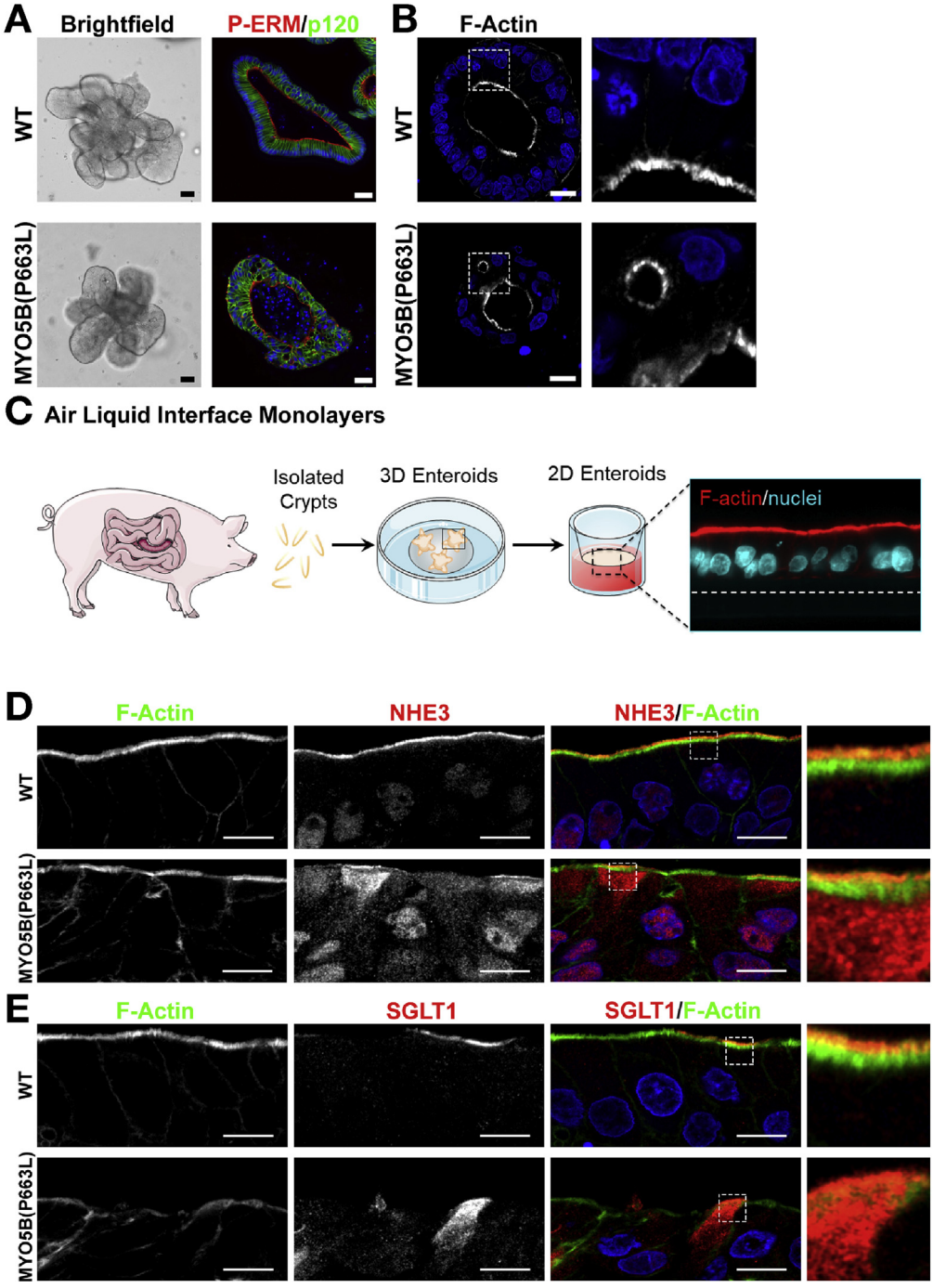

Figure 4. Pig MYO5B(P663L) enteroids mimic in vivo findings. (*A*) Brightfield image of WT and MYO5B(P663L) 3D enteroids appeared similar. Immunofluorescence staining for P-ERM and p120 showed disorganized cell structure in MYO5B(P663L) enteroids and aberrant expression of P-ERM. (*B*) F-actin staining showed the presence of subapical inclusions in MYO5B(P663L)-derived enteroids. (*C*) Schematic of the development of 2D enteroid monolayer cultured using air–liquid interface. (*D*) Immunostaining of enteroid monolayers demonstrated well-developed brush border in WT enterocytes that expressed NHE3 on the apical membrane. Cultured MYO5B(P663L) enterocytes appeared disorganized with subapical accumulation of NHE3. (*E*) SGLT1 immunostaining showed apical expression in many WT enterocytes. In MYO5B(P663L) enterocytes SGLT1 was observed diffusely below the apical membrane. Scale bars: 50 μm in (*A*), 2 μm in (*B*), 10 μm in (*C*, *D*).

MYO5B.[41,42] In MYO5B(P663L) liver hepatocytes, we observed thickened and irregular canalicular and cytoplasmic staining of BSEP compared to WT hepatocytes (Figure 7*A*). Immunostaining for MRP2 showed subtle alterations with increased thickness of the canalicular membrane in MYO5B(P663L) hepatocytes, but without the cytoplasmic localization seen for BSEP (Figure 7*B*). The localization of MRP2 in MYO5B(P663L) pigs is consistent with previous reports in patients with MVID who exhibited cholestasis.[41] Immunostaining for BSEP and MRP2 demonstrate alterations in canalicular morphology in MYO5B(P663L) pigs compared to WT, indicative of a role for MYO5B in the proper formation and delivery of BSEP to the canalicular membrane.

Discussion

A porcine model of MVID exhibits large changes in intestinal epithelium, which are accompanied by alterations in BSEP expression in the liver. We demonstrate that the P663L mutation in MYO5B results in altered localization of MYO5B in the intestine and liver. Proper localization of

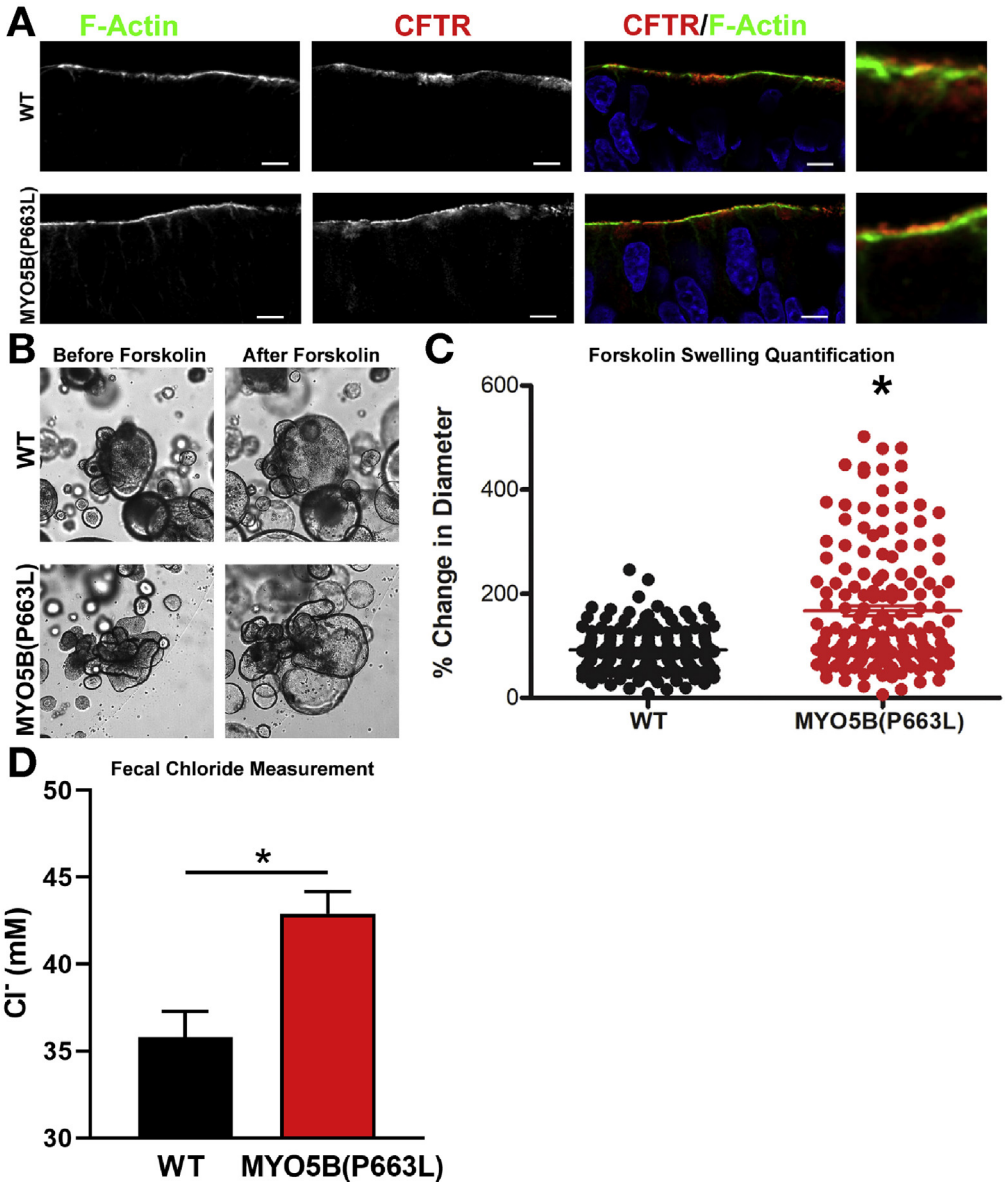

Figure 5. Functional CFTR in MYO5B(P663L) enteroids. (*A*) In enteroid monolayers cultured using an air–liquid interface CFTR was observed on the apical membrane of MYO5B(P663L) enterocytes. (*B*) *Brightfield micrograph* of differentiated WT and MYO5B(P663L) pig-derived 3D enteroids before and 1 hour after administration of forskolin. (*C*) Forskolin swelling, measured as percent change in diameter, after 1-hour forskolin administration. MYO5B(P663L) swelled to a greater degree compared with WT enteroids. $^{*}P < .05$, n = 155 WT, n = 156 MYO5B(P663L) enteroids, performed in 3 separate experiments. (*D*) Fecal chloride measures from WT and MYO5B(P663L) piglets as determined by a chloride probe performed in triplicate.

MYO5B is likely critical for the proper trafficking and anchoring of brush border components. Previous studies suggest that MYO5B serves as a processive anchor, localizing vesicles and their cargoes to the subapical brush border.[45] In MYO5B(P663L) pigs, MYO5B was predominantly localized in close proximity to the Golgi apparatus, with little subapical MYO5B. In human MVID patients with the Navajo MYO5B P660L mutation, a similar distribution of cytoplasmic MYO5B was observed, suggesting that this pig model may closely mimic human MVID. Our data in humans and pigs demonstrate that with the human P660L or pig P663L mutation in MYO5B, MYO5B is concentrated in the cytosol of enterocytes, a pattern distinct from WT MYO5B. In the liver, the altered location of MYO5B in pig hepatocytes is more subtle between WT and MYO5B(P663L) hepatocytes. In MYO5B(P663L) pig liver, MYO5B is still located relatively near the canalicular membrane, although it appears to be more focally concentrated in the cytoplasm compared to WT. This may in part explain why individuals with MVID present with profound intestinal abnormalities immediately after birth, while liver cholestasis manifests later in life.

MYO5B(P663L) pigs showed pronounced villus blunting and cell rounding in the small intestine by electron microscopy, suggesting that MYO5B is crucial for proper villi formation. Villus atrophy and villus blunting have been reported in individuals maintained without enteral feeding,[46–50] raising the possibility that in MVID biopsies, this observation may not be the direct result of MYO5B mutation. Neonatal mouse models of MVID have not reported pronounced cell rounding at the tips of villi or stunting of villi.[15–17] However, these intestinal aberrations have been well documented in patients with MVID.[24,27,28,31] The cell rounding observed by scanning electron microscopy in

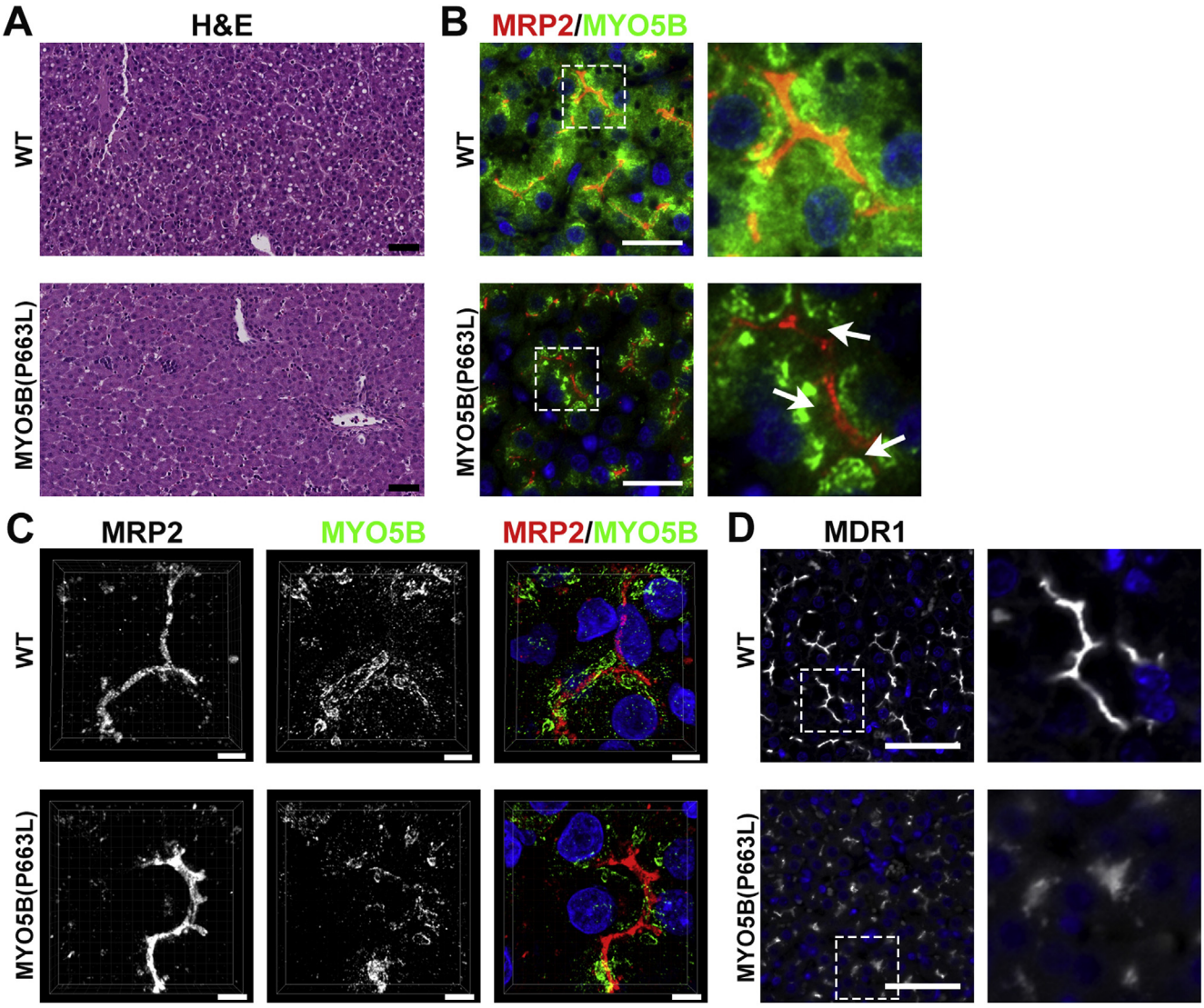

Figure 6. Expression of MYO5B and MDR1 in WT and MYO5B(P663L) hepatocytes. (*A*) H&E of WT and MYO5B(P663L) pig liver showed the presence of lipid droplets in WT hepatocytes, but no other difference was observed. Scale bars: 50 μm. (*B*, *C*) In WT pigs, MYO5B appeared closely associated with the canalicular membrane, delineated by MRP2 immunostaining. MYO5B also appeared throughout the cytoplasm of hepatocytes. In MYO5B(P663L) hepatocytes MYO5B appeared in dense clusters more distant from the canalicular membrane compared to WT hepatocytes, distance of MYO5B from MRP2 is indicated by *arrows*. Less cytoplasmic MYO5B was observed in MYO5B(P663L) pigs compared to WT pigs. Scale bars: 50 μm and 5 μm, respectively. (*D*) MDR1 in WT and MYO5B(P663L) hepatocytes demonstrated decreased expression of MDR1 in MYO5B(P663L) hepatocytes compared with WT. MDR1 appeared diffusely below the canalicular membrane in MYO5B(P663L) hepatocytes.

patients with MVID reported by Cutz et al[27] is remarkably similar to our observations in MYO5B(P663L) pigs. While germline Myo5b KO mice lack prominent cell rounding, the dominant negative mutation in the P660L (P663L in pigs) mutation may elicit a greater impact on intestinal epithelium than knockout of MYO5B. Our pig model of MVID supports a role for MYO5B in maintenance or development of intestinal villi structure. TEM showed large gaps existing between intestinal cells in MYO5B(P663L) duodenum compared to WT duodenum. Additionally, lateral microvilli were observed between intestinal cells in MYO5B(P663L) pigs by TEM. The presence of lateral microvilli has been reported in intestinal tissue from patients with MVID by TEM.[28,30,51] It has been contentious whether fluid absorbed by enterocytes flows back into the intestinal lumen through the paracellular pathway in MVID patients. Mouse models of MVID suggested that junctional changes between intestinal cells may be the result of TPN.[14] However, MYO5B(P663L) pig intestine suggests that profound changes in cell to cell adhesion that result from the P663L mutation early in development may contribute to MVID-associated diarrhea.

The germline Myo5b KO mouse developed in our laboratory showed the most profound intestinal abnormalities in the proximal small intestine, which included increased

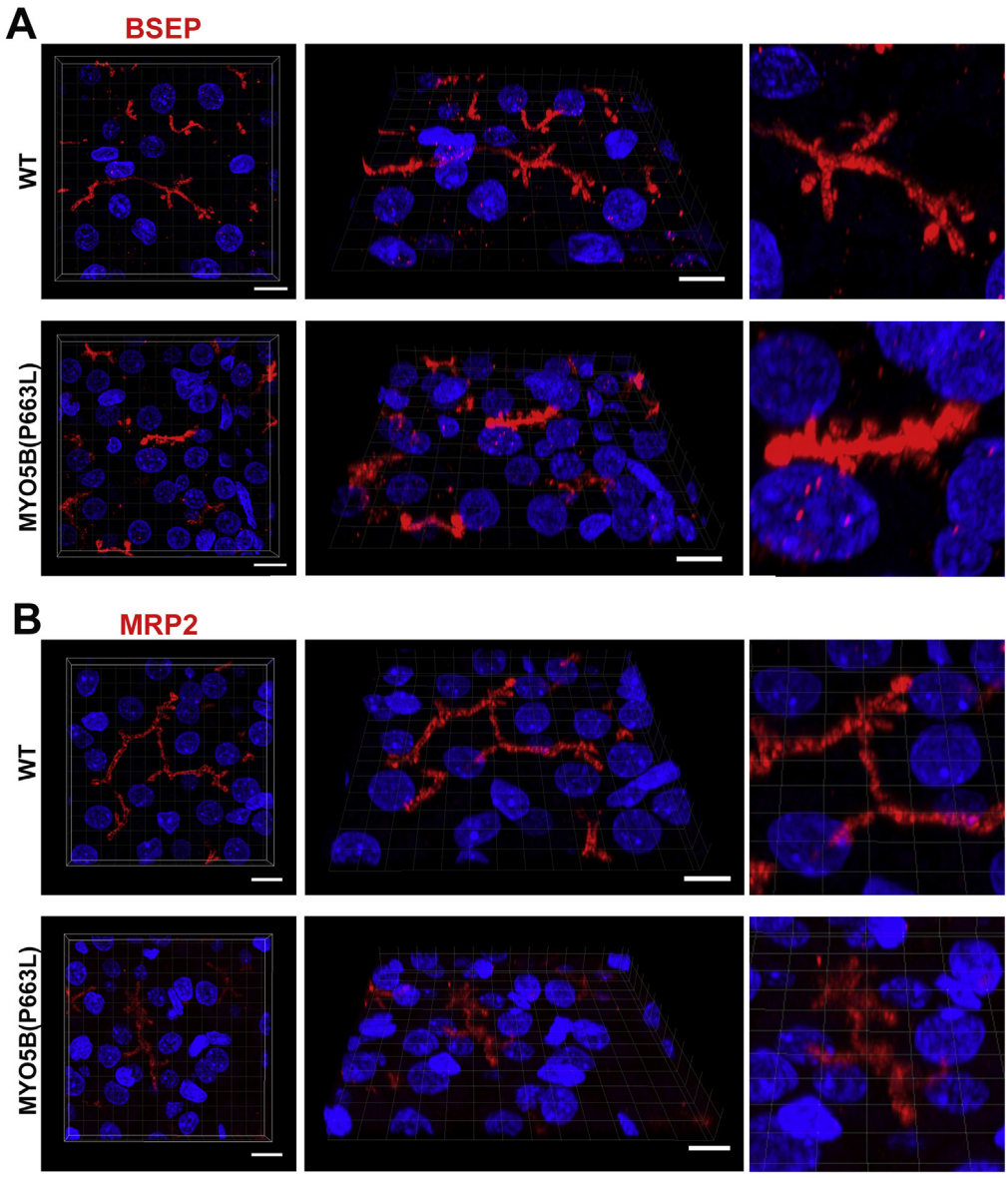

Figure 7. MYO5B(P663L) pigs exhibit alterations in BSEP localization in hepatocytes. (*A*) Z-stack projections of WT liver showed well-developed canaliculi with apical BSEP localization. MYO5B(P663L) presented canaliculi that appeared stunted and thickened with BSEP present below the canalicular membrane in hepatocytes. (*B*) MRP2 was observed on the canalicular membrane of WT and MYO5B(P663L) hepatocytes, however, MYO5B(P663L) hepatocyte canaliculi appeared less developed. Scale bars: 10 μm.

frequency of inclusions and fused villi.[17] Due to the limited availability of tissue samples from the different segments of the intestine from the same patient with MVID, it has been difficult to determine whether individuals with MVID have a less severe intestinal phenotype in the distal small intestine. Examination of the small intestine of MYO5B(P663L) pigs demonstrated similar numbers of inclusions along the whole length of the small intestine, as well as subapical accumulation of NHE3 and CD10 in the ileum. The distal small intestine did not show any abatement of mislocalization of brush border components, suggesting that inherent differences exist between mouse Myo5b KO models of MVID and the MYO5B(P663L) pig model of MVID. These data also suggest that patients with MVID likely have alterations in transporter localization that persist along the length of the small and large intestines.

The mislocalization of sodium transporters, which showed loss of apical expression in the brush border and intracellular accumulation, closely recapitulates in vivo findings in MVID mouse models, as well as immunostaining reports in human MVID patients.[12,14,17,33,52] In MYO5B(P663L) pigs, SGLT1 was dramatically reduced on the apical membrane and large amounts of SGLT1 were observed below the brush border compared to WT pigs. SGLT1 is the primary transporter responsible for Na^+-dependent sugar transport and is estimated to account for the absorption of 5 L of water per day in the small intestine of adult humans.[53,54] NHE3 also demonstrated decreased apical expression, as well as intracellular accumulation in MYO5B(P663L) pigs compared to WT enterocytes. NHE3 is the major sodium hydrogen exchanger in the intestinal brush border and is responsible for the majority of intestinal Na^+ absorption, which facilitates net fluid absorption. Recessive *SLC9A3* mutations, which result in absent or mutated NHE3 protein, cause congenital sodium diarrhea in humans.[55] The decreased expression of both SGLT1 and NHE3, which are responsible for a large proportion of

Na^+-dependent water absorption in the small and large intestines, may explain the severe diarrhea observed in our pig model of MVID and in MVID patients. In support of this concept, MVID patients have high concentrations of fecal Na^+, suggesting defects in sodium absorption.[36]

The mislocalization of NHE3 and SGLT1 likely stems from improper trafficking of NHE3 and SGLT1 to the apical membrane. While apical proteins are often present in inclusions, inclusions are the result of endocytosis of the apical membrane and are not the primary cause of MVID-associated diarrhea.[56] This was demonstrated by inhibition of inclusion formation by knocking out Pacsin 2 (Syndapin 2) in vivo in Myo5b KO mice, which results in rare inclusions. Still, SGLT1 apical localization is severely decreased in these mice, which die early in development and have watery stool. Additionally, adult inducible intestine-specific VillinCre^{ERT2};Myo5b$^{flox/flox}$ mice that lack Myo5b have few inclusions, but still have significantly decreased apical NHE3 and SGLT1 and severe diarrhea.[14] Therefore, the improper delivery of apical proteins resulting from mutations in MYO5B, rather than inclusions, is likely the primary contributor to decreased apical localization of NHE3 and SGLT1.

In contrast to the loss of apical sodium transporters, CFTR was largely maintained at the apical membrane of enterocytes and increased swelling was observed in MYO5B(P663L) enteroids in response to forskolin. Consistent with these findings, we previously reported that, in tamoxifen-induced VillinCre^{ERT2};Myo5b$^{flox/flox}$ mice, CFTR contributes to basal and stimulated I_{sc} to a greater degree than in tamoxifen-treated control mice.[14] Rhoads et al[57] previously reported in human jejunal tissue from MVID patients that chloride secretion was near the maximal rate of healthy tissue. T84 cells with knockdown of MYO5B did not affect CFTR ion transport and CFTR was expressed in the brush border of Caco2 cells with MYO5B knockdown.[31,33] Furthermore, CFTR was observed on the apical membrane in human MVID intestinal tissue.[14,33] Forteza and colleagues[58] reported that MYO5B loss of function and exposure of intestinal epithelium to glucocorticoids at birth results in PKA stimulation that drives CFTR-mediated Cl^- secretion and thus secretory diarrhea. These data suggest that active chloride secretion mediated through CFTR may be occurring in MVID, further driving dehydration that likely results from mislocalization of sodium transporters.

Cholestasis in patients with MVID was previously presumed to result from long-term TPN alimentation, which is a known risk factor in individuals with intestinal failure.[7,8,59,60] Our large animal model of MVID suggests that early alterations in canalicular membrane protein expression (BSEP and MDR1) result from mutation in MYO5B. In support of these findings, 2 groups have recently reported that individuals with mutations in MYO5B that have never received parenteral nutrition and do not present recurrent diarrhea, develop intrahepatic cholestasis.[42,43] Patients with cholestasis who harbor a mutation in MYO5B have an abnormal distribution of BSEP with subapical expression below the canalicular membrane.[42,43] Gonzales et al[43] also reported thickened canalicular staining similar to our findings in MYO5B(P663L) hepatocytes. In patients with MVID, cholestasis has been linked to inherent loss of function of MYO5B accompanied by decreased apical BSEP and not TPN alimentation.[41,61] In MYO5B(P663L) pig liver, we observed altered expression of MYO5B, which has also been reported in hepatocytes of patients with isolated cholestasis, who have mutations in MYO5B, and in MVID patients who develop cholestasis.[41–43] Additionally, Overeem et al[62] has recently found that mutant MYO5B(P660L) causes the intracellular accumulation of bile canaliculi resident proteins in hepatocyte HEPG2 and HUES9 cells.

In summary, we have examined the effects of the P663L mutation in MYO5B in genetically engineered neonatal pigs. Our findings demonstrate that the Navajo mutation in MYO5B results in intestinal abnormalities that persist along the length of the small and large intestines and include villus atrophy, inclusions, alterations in apical transporters, and mislocalization of MYO5B. Moreover, this large animal model of MVID documents early changes in hepatocyte canalicular membrane formation and expression of BSEP that likely contribute to the cholestasis associated with MVID. While the development of a pig model for MVID was expensive and required cloning of piglets from engineered fibroblasts, the close correlation of pathology in the pigs with those in Navajo MVID patients indicates that significant insights into human disease can be gleaned from pig models. Our findings suggest that development of therapeutic treatments that correct trafficking of sodium transporters to the apical membrane and inhibit chloride secretion through CFTR may help ameliorate MVID-associated diarrhea.

Supplementary Material

Note: To access the supplementary material accompanying this article, visit the online version of *Gastroenterology* at www.gastrojournal.org, and at https://doi.org/10.1053/j.gastro.2020.02.034.

References

1. Muller T, Hess MW, Schiefermeier N, et al. MYO5B mutations cause microvillus inclusion disease and disrupt epithelial cell polarity. Nat Genet 2008;40:1163–1165.
2. Ruemmele FM, Muller T, Schiefermeier N, et al. Loss-of-function of MYO5B is the main cause of microvillus inclusion disease: 15 novel mutations and a CaCo-2 RNAi cell model. Hum Mutat 2010;31:544–551.
3. Erickson RP, Larson-Thome K, Valenzuela RK, et al. Navajo microvillous inclusion disease is due to a mutation in MYO5B. Am J Med Genet A 2008;146A:3117–3119.
4. Al-Sinani S, Sharef SW, Lakhtakia R, et al. Diagnosis of microvillous inclusion disease: a case report and literature review with significance for oman. Oman Med J 2012;27:497–500.
5. Perry A, Bensallah H, Martinez-Vinson C, et al. Microvillous atrophy: atypical presentations. J Pediatr Gastroenterol Nutr 2014;59:779–785.

6. Siahanidou T, Koutsounaki E, Skiathitou AV, et al. Extraintestinal manifestations in an infant with microvillus inclusion disease: complications or features of the disease? Eur J Pediatr 2013;172:1271–1275.
7. Teitelbaum DH. Parenteral nutrition-associated cholestasis. Curr Opin Pediatr 1997;9:270–275.
8. Farrell MK, Balistreri WF. Parenteral nutrition and hepatobiliary dysfunction. Clin Perinatol 1986;13:197–212.
9. Comegna M, Amato F, Liguori R, et al. Two cases of microvillous inclusion disease caused by novel mutations in MYO5B gene. Clin Case Rep 2018;6:2451–2456.
10. Pohl JF, Shub MD, Trevelline EE, et al. A cluster of microvillous inclusion disease in the Navajo population. J Pediatr 1999;134:103–106.
11. Kravtsov D, Mashukova A, Forteza R, et al. Myosin 5b loss of function leads to defects in polarized signaling: implication for microvillus inclusion disease pathogenesis and treatment. Am J Physiol Gastrointest Liver Physiol 2014;307:G992–G1001.
12. Knowles BC, Roland JT, Krishnan M, et al. Myosin Vb uncoupling from RAB8A and RAB11A elicits microvillus inclusion disease. J Clin Invest 2014;124:2947–2962.
13. Thoeni CE, Vogel GF, Tancevski I, et al. Microvillus inclusion disease: loss of Myosin vb disrupts intracellular traffic and cell polarity. Traffic 2014;15:22–42.
14. Engevik AC, Kaji I, Engevik MA, et al. Loss of MYO5B Leads to reductions in Na(+) absorption with maintenance of CFTR-dependent Cl(-) secretion in enterocytes. Gastroenterology 2018;155:1883–1897e10.
15. Carton-Garcia F, Overeem AW, Nieto R, et al. Myo5b knockout mice as a model of microvillus inclusion disease. Sci Rep 2015;5:12312.
16. Schneeberger K, Vogel GF, Teunissen H, et al. An inducible mouse model for microvillus inclusion disease reveals a role for myosin Vb in apical and basolateral trafficking. Proc Natl Acad Sci U S A 2015;112:12408–12413.
17. Weis VG, Knowles BC, Choi E, et al. Loss of MYO5B in mice recapitulates microvillus inclusion disease and reveals an apical trafficking pathway distinct to neonatal duodenum. Cell Mol Gastroenterol Hepatol 2016;2:131–157.
18. Doyle EL, Booher NJ, Standage DS, et al. TAL effector-nucleotide targeter (TALE-NT) 2.0: tools for TAL effector design and target prediction. Nucleic Acids Res 2012;40:W117–W122.
19. Bedell VM, Wang Y, Campbell JM, et al. In vivo genome editing using a high-efficiency TALEN system. Nature 2012;491:114118.
20. Carlson DF, Tan W, Lillico SG, et al. Efficient TALEN-mediated gene knockout in livestock. Proc Natl Acad Sci U S A 2012;109:17382–17387.
21. Tan W, Carlson DF, Lancto CA, et al. Efficient nonmeiotic allele introgression in livestock using custom endonucleases. Proc Natl Acad Sci U S A 2013;110:16526–16531.
22. Tan WS, Carlson DF, Walton MW, et al. Precision editing of large animal genomes. Adv Genet 2012;80:37–97.
23. Carlson DF, Fahrenkrug SC, Hackett PB. Targeting DNA with fingers and TALENs. Mol Ther Nucleic Acids 2012;1:e3.
24. Davidson GP, Cutz E, Hamilton JR, et al. Familial enteropathy: a syndrome of protracted diarrhea from birth, failure to thrive, and hypoplastic villus atrophy. Gastroenterology 1978;75:783–790.
25. Groisman GM, Sabo E, Meir A, et al. Enterocyte apoptosis and proliferation are increased in microvillous inclusion disease (familial microvillous atrophy). Hum Pathol 2000;31:1404–1410.
26. Lake BD. Microvillus inclusion disease: specific diagnostic features shown by alkaline phosphatase histochemistry. J Clin Pathol 1988;41:880–882.
27. Cutz E, Rhoads JM, Drumm B, et al. Microvillus inclusion disease: an inherited defect of brush-border assembly and differentiation. N Engl J Med 1989;320:646–651.
28. Phillips AD, Schmitz J. Familial microvillous atrophy: a clinicopathological survey of 23 cases. J Pediatr Gastroenterol Nutr 1992;14:380–396.
29. Croft NM, Howatson AG, Ling SC, et al. Microvillous inclusion disease: an evolving condition. J Pediatr Gastroenterol Nutr 2000;31:185–189.
30. Iancu TC, Mahajnah M, Manov I, et al. Microvillous inclusion disease: ultrastructural variability. Ultrastruct Pathol 2007;31:173–188.
31. Ameen NA, Salas PJ. Microvillus inclusion disease: a genetic defect affecting apical membrane protein traffic in intestinal epithelium. Traffic 2000;1:76–83.
32. Kiela PR, Ghishan FK. Physiology of intestinal absorption and secretion. Best Pract Res Clin Gastroenterol 2016;30:145–159.
33. Kravtsov DV, Ahsan MK, Kumari V, et al. Identification of intestinal ion transport defects in microvillus inclusion disease. Am J Physiol Gastrointest Liver Physiol 2016;311:G142–G155.
34. Gabriel SE, Brigman KN, Koller BH, et al. Cystic fibrosis heterozygote resistance to cholera toxin in the cystic fibrosis mouse model. Science 1994;266:107–109.
35. Li C, Dandridge KS, Di A, et al. Lysophosphatidic acid inhibits cholera toxin-induced secretory diarrhea through CFTR-dependent protein interactions. J Exp Med 2005;202:975–986.
36. Ruemmele FM, Schmitz J, Goulet O. Microvillous inclusion disease (microvillous atrophy). Orphanet J Rare Dis 2006;1:22.
37. Youssef N, F.M.R., Goulet O, et al. [CD10 expression in a case of microvillous inclusion disease]. Ann Pathol 2004;24:624–627.
38. Groisman GM, Amar M, Livne E. CD10: a valuable tool for the light microscopic diagnosis of microvillous inclusion disease (familial microvillous atrophy). Am J Surg Pathol 2002;26:902–907.
39. Dekkers JF, Wiegerinck CL, de Jonge HR, et al. A functional CFTR assay using primary cystic fibrosis intestinal organoids. Nat Med 2013;19:939–945.
40. Foulke-Abel J, In J, Kovbasnjuk O, et al. Human enteroids as an ex-vivo model of host-pathogen interactions in the gastrointestinal tract. Exp Biol Med (Maywood) 2014;239:1124–1134.
41. Girard M, Lacaille F, Verkarre V, et al. MYO5B and bile salt export pump contribute to cholestatic liver disorder

in microvillous inclusion disease. Hepatology 2014; 60:301–310.
42. Qiu YL, Gong JY, Feng JY, et al. Defects in myosin VB are associated with a spectrum of previously undiagnosed low gamma-glutamyltransferase cholestasis. Hepatology 2017;65:1655–1669.
43. Gonzales E, Taylor SA, Davit-Spraul A, et al. MYO5B mutations cause cholestasis with normal serum gamma-glutamyl transferase activity in children without microvillous inclusion disease. Hepatology 2017;65:164–173.
44. Keppler D. Cholestasis and the role of basolateral efflux pumps. Z Gastroenterol 2011;49:1553–1557.
45. Schafer JC, Baetz NW, Lapierre LA, et al. Rab11-FIP2 interaction with MYO5B regulates movement of Rab11a-containing recycling vesicles. Traffic 2014;15:292–308.
46. Feng Y, Teitelbaum DH. Epidermal growth factor/TNF-alpha transactivation modulates epithelial cell proliferation and apoptosis in a mouse model of parenteral nutrition. Am J Physiol Gastrointest Liver Physiol 2012; 302:G236–G249.
47. Buchman AL, Moukarzel AA, Bhuta S, et al. Parenteral nutrition is associated with intestinal morphologic and functional changes in humans. JPEN J Parenter Enteral Nutr 1995;19:453–460.
48. Pironi L, Paganelli GM, Miglioli M, et al. Morphologic and cytoproliferative patterns of duodenal mucosa in two patients after long-term total parenteral nutrition: changes with oral refeeding and relation to intestinal resection. JPEN J Parenter Enteral Nutr 1994;18:351–354.
49. Shaw D, Gohil K, Basson MD. Intestinal mucosal atrophy and adaptation. World J Gastroenterol 2012;18:6357–6375.
50. Ney DM. Effects of insulin-like growth factor-I and growth hormone in models of parenteral nutrition. JPEN J Parenter Enteral Nutr 1999;23:S184–S189.
51. Morroni M, Cangiotti AM, Guarino A, et al. Unusual ultrastructural features in microvillous inclusion disease: a report of two cases. Virchows Arch 2006;448:805–810.
52. Vogel GF, Janecke AR, Krainer IM, et al. Abnormal Rab11-Rab8-vesicles cluster in enterocytes of patients with microvillus inclusion disease. Traffic 2017;18:453–464.
53. Wright E, Loo D, Hirayama B, et al. Sugar Absorption Physiology of the Gastrointestinal Tract: Physiology of the Gastrointestinal Tract. 4th ed. New York: Elsevier, 2006.
54. Hirschhorn N, Kinzie JL, Sachar DB, et al. Decrease in net stool output in cholera during intestinal perfusion with glucose-containing solutions. N Engl J Med 1968; 279:176–181.
55. Janecke AR, Heinz-Erian P, Yin J, et al. Reduced sodium/proton exchanger NHE3 activity causes congenital sodium diarrhea. Hum Mol Genet 2015;24:6614–6623.
56. Engevik AC, Kaji I, Postema MM, et al. Loss of myosin Vb promotes apical bulk endocytosis in neonatal enterocytes. J Cell Biol 2019;218:3647–3662.
57. Rhoads JM, Vogler RC, Lacey SR, et al. Microvillus inclusion disease. In vitro jejunal electrolyte transport. Gastroenterology 1991;100:811–817.
58. Forteza R, Ahsan MK, Carton-Garcia F, et al. Glucocorticoids and Myosin5b loss-of-function induce heightened PKA signaling in addition to membrane traffic defects. Mol Biol Cell 2019mbcE18070415.
59. Lauriti G, Zani A, Aufieri R, et al. Incidence, prevention, and treatment of parenteral nutrition-associated cholestasis and intestinal failure-associated liver disease in infants and children: a systematic review. JPEN J Parenter Enteral Nutr 2014;38:70–85.
60. Rangel SJ, Calkins CM, Cowles RA, et al. Parenteral nutrition-associated cholestasis: an American Pediatric Surgical Association Outcomes and Clinical Trials Committee systematic review. J Pediatr Surg 2012;47:225–240.
61. **Schlegel C, Weis VG, Knowles BC**, et al. Apical membrane alterations in non-intestinal organs in microvillus inclusion disease. Dig Dis Sci 2018;63:356–365.
62. Overeem AW, Li Q, Qiu YL, et al. A molecular mechanism underlying genotype-specific intrahepatic cholestasis resulting from MYO5B mutations. Hepatology 2019 Nov 21 [Epub ahead of print].

Author names in bold designate shared co-first authorship.

Received November 20, 2019. Accepted February 17, 2020.

Correspondence
Address correspondence to: Amy C. Engevik, PhD, Epithelial Biology Center, Vanderbilt University Medical Center, 10435 Medical Research Building IV, 2213 Garland Avenue, Nashville, Tennessee 37232. e-mail: amy.c.engevik@vumc.org; fax: 615-343-1591.

Acknowledgments
The authors thank Christopher R. Marino, University of Tennessee, Memphis for the CFTR antibody R3194 (listed in Supplementary Table 1).

CRediT Authorship Contributions
Amy C. Engevik, PhD (Conceptualization: Supporting; Data curation: Lead; Formal analysis: Lead; Methodology: Equal; Writing – original draft: Lead; Writing – review & editing: Lead). Alexander W. Coutts, BS (Conceptualization: Supporting; Data curation: Supporting; Methodology: Supporting; Writing – original draft: Supporting). Izumi Kaji, PhD (Data curation: Supporting; Methodology: Supporting). Paula Rodriguez, DVM, PhD, MVSc (Methodology: Supporting; Resources: Supporting; Writing – review & editing: Supporting). Felipe Ongaratto, DVM, PhD (Investigation: Supporting; Methodology: Supporting; Writing – review & editing: Supporting). Milena Saqui-Salces, PhD (Conceptualization: Supporting; Data curation: Supporting; Methodology: Supporting). Ramya Lekha Medida, BS (Data curation: Supporting; Methodology: Supporting). Anne R. Meyer, BS (Data curation: Supporting; Methodology: Supporting). Elena Kolobova, PhD (Data curation: Supporting; Methodology: Supporting). Melinda A. Engevik, PhD (Methodology: Supporting; Writing – review & editing: Supporting). Janice A. Williams, PhD (Data curation: Supporting; Methodology: Supporting). Mitchell D. Shub, MD (Data curation: Supporting; Resources: Supporting). Daniel F. Carlson, PhD (Data curation: Supporting; Resources: Supporting). Tamene Melkamu, PhD (Conceptualization: Equal; Data curation: Supporting; Methodology: Supporting; Writing – review & editing: Supporting). James R. Goldenring, MD, PhD (Conceptualization: Supporting; Data curation: Supporting; Funding acquisition: Lead; Investigation: Lead; Methodology: Supporting; Resources: Lead; Supervision: Lead; Writing – original draft: Supporting; Writing – review & editing: Supporting).

Conflicts of interest
The authors disclose no conflicts.

Funding
This work was supported by the National Institute of Health (NIH) grants R43 DK109820 to Tamene Melkamu and James R. Goldenring, R01 DK48370, R01 DK70856 and a gift from the Christine Volpe Fund to James R. Goldenring. Amy C. Engevik was supported by NIH F32 DK111101 and KO1 DK12186901. This work was supported by core resources of the Vanderbilt Digestive Disease Center (P30 DK058404), the Vanderbilt-Ingram Cancer Center (P30 CA68485), and imaging supported by both the Vanderbilt Cell Imaging Shared Resource and the Vanderbilt Digital Histology Shared Resource (supported by a VA Shared Equipment Grant 1IS1BX003097).

Supplementary Methods

Frozen Section Immunostaining

Fixed tissue was embedded in OCT and stored at −80°C before sectioning. Five-micrometer sections were cut using a cryotome. Slides were incubated in phosphate-buffered saline (PBS) for 15 minutes before staining to remove OCT. Sections were permeabilized with 0.3% Triton X-100 and blocked for 1 hour at room temperature in 10% donkey serum. Slides were then washed for 5 minutes in PBS. Primary antibodies were diluted in 1% donkey serum and 0.05% Tween 20 in PBS overnight in a humidified chamber at 4°C. Slides were washed 3 times in PBS for 5 minutes before addition of secondary antibodies. Secondary antibodies along with fluorescently labeled phalloidin were incubated for 1 hour at room temperature. Secondary antibodies were diluted 1:200 in PBS, phalloidin was added 1:100 in PBS to visualize the actin rich brush border. Hoechst diluted 1:1000 in PBS was added to each section for 5 minutes to stain nuclei. Slides were washed 3 times for 5 minutes and coverslipped using Prolong Gold Antifade.

Imaging

All immunofluorescence images were acquired using a Zeiss Axio Imager microscope equipped with an Axiovision digital imaging system using a 20× or 40× objective or a Zeiss Confocal LSM 880 using 63× objective with Airyscan detector. The Axio 20× and 40× objective were, respectively, a Plan-apochromat with a numerical aperture of 0.8 M27 or 0.95 Korr M27. The Axio Imager microscope was equipped with an AxioCam HRm Rev.3. The LSM 880 63× objective had a numerical aperture of 1.4.

MYO5B Mean Fluorescence Intensity Quantification

Five 20× images at a fixed exposure were taken of MYO5B-immunostained duodenum tissue from WT and MYO5B(P663L) pigs to determine whether levels of MYO5B protein were reduced in MYO5B(P663L) pigs compared to WT. Fiji (ImageJ) software was used to measure the mean fluorescence intensity of MYO5B in cells. The region above the nucleus, including the brush border, was measured in 100 cells per field of view for a total of 500 cells measured per pig.

Electron Microscopy

Small pieces of intestinal tissue were excised and prepared for TEM and scanning electron microscopy (SEM) by fixing in 2.5% glutaraldehyde in 0.1 mol/L cacodylate buffer at room temperature for 1 hour followed by overnight fixation at 4°C. Samples were washed and incubated with 1% osmium tetroxide for 1 hour, followed by ethanol dehydration (30%, 50%, 70%, 95%, and 100%). For TEM, samples were further dehydrated in propylene oxide. After dehydration, tissue pieces were infiltrated with and embedded in EPON 812 resin (cat no. 14120; Electron Microscopy Sciences, Hatfield, PA). The ultrathin sections (60–70 nm) were placed on 300 mesh copper grids. Sections were stained with 2% uranyl acetate followed by Reynold's lead citrate. Images were acquired using a Philips/FEI T-12 Tecnai electron microscope. For SEM, the dehydrated samples were dried using hexamethyldisilazane, mounted on stubs and sputter coated with gold/palladium. A FEI Quanta 250 scanning electron microscope was used to obtain SEM images.

Crypt Isolation and Enteroid Generation

After excision, the duodenum was opened lengthwise, washed in PBS without Ca^{2+} and Mg^{2+} and cut into approximately 20-mm segments. The intestinal pieces were washed again until the supernatant was clear and then placed in 30 mL of advanced Dulbecco's modified Eagle medium (DMEM)/F12 containing collagenase (1 mg/mL) and bovine serum albumin (2 mg/mL) for 30 minutes at 37°C with shaking. After 30 minutes, a 3-mL transfer pipette was used to gently remove villi and crypts from the pieces of intestine. Fifty microliters of supernatant was examined using an inverted microscope to determine quality and quantity of crypts isolated. The supernatant containing villi and crypts was passed through a 70-μm filter to remove the villi. The flow through containing intestinal crypts was then centrifuged at 300*g* for 5 minutes. The resulting pellet was resuspended in Matrigel and 30 μL of Matrigel suspension containing crypts were aliquoted per well in a 48-well plate. The plate was incubated at 37°C for 15 minutes to facilitate Matrigel polymerization and then overlaid with 300 μL of prewarmed Human IntestiCult (cat. no. 06010; Stem Cell Technologies, Vancouver, Canada) media containing penicillin/streptomycin. Media were changed every other day and resulting enteroids were passaged every 5–7 days. To passage enteroids medium was removed from wells and each well containing a Matrigel dome was gently resuspended in 1 mL of organoid harvesting solution (no. 3700-100-01; Trevigen, Gaithersburg, MD). Wells were placed on a shaker at 4°C for 15–20 minutes to facilitate removal of Matrigel. Like wells were then pooled into a 15-mL tube and centrifuged at 300*g* for 5 minutes. Medium was aspirated and enteroids were resuspended in 1 mL of TrypLE Express (cat. no. 12604013; Thermo Fisher Scientific) and incubated at 37°C for 3 minutes. The TrypLE solution was triturated 10 times to reduce enteroids to small clumps of cells. Ten milliliters of DMEM were added to inactivate TrypLE before centrifugation at 300*g* for 5 minutes. TrypLE and DMEM solution was removed and enteroid fragments were resuspended in Matrigel. After Matrigel was polymerized at 37°C (approximately 15 minutes) each dome of Matrigel was overlaid with 300 μL of prewarmed human Intesticult media.

Enteroid Monolayers Cultured Using Air–Liquid Interface

To generate 2D monolayers of pig enteroids, 3D enteroids were used approximately 5 days after passaging; 2.5

μL of Matrigel was added to 100 μL of ice-cold PBS without Ca^{2+} and Mg^{2+} and the solution was added to the apical surface of each Transwell. Transwells containing Matrigel in PBS were incubated at 37°C for 1.5 hours. Generally, 2 wells containing 75 enteroids per well were used to generate one 6.5-mm Transwell (no. 3470; Corning). Five days after passaging, 3D enteroids were resuspended in 1 mL of organoid harvesting solution to de-polymerize the extracellular matrix and placed at 4°C on a shaker for 15–20 minutes. After Matrigel de-polymerization replicate wells were pooled and centrifuged at 300*g* for 5 minutes. The organoid harvesting solution was removed and the pellet of enteroids was resuspended in 1 mL of TrypLE Express solution to dissociate enteroids. Enteroids were incubated for 5 minutes at 37°C in TrypLE Express. Next, 1 mL of DMEM was added to the enteroids, followed by trituration with a 1-mL pipette, until a single-cell suspension was achieved. Ten milliliters of DMEM was added to inactivate TrypLE. Cells were centrifuged at 300*g* for 5 minutes. During centrifugation, the Transwell plate containing Matrigel in PBS was removed from the incubator and the solution was removed from each Transwell. The plate was briefly dried in the hood with the lid removed. After centrifugation, the pellet was resuspended in human Intesticult and 100 μL of the cell suspension were added to the top of each Transwell. Six hundred microliters of human Intesticult was added to the bottom of each Transwell and the plate was incubated at 37°C. Human Intesticult media was replaced after 2 days. For the air–liquid interface, the following day (day 3 since 2D plating) the human Intesticult media from the apical domain was removed and the human Intesticult from the basolateral domain was replaced with differentiation media, lacking Wnt. The basolateral differentiation media was replaced on day 5 and any fluid that was present on the apical domain was also removed. On day 7, monolayers were fixed in either 4% paraformaldehyde or 10% neutral buffered formalin for 30 minutes at room temperature. Monolayers were washed in PBS for 5 minutes. For cryoprotection, 30% sucrose in PBS solution was added to each Transwell for 3 hours and then monolayers were embedded in OCT.

Forskolin Swelling Assay

Differentiated 3D enteroids from WT and MYO5B(P663L) pigs were analyzed to determine CFTR function in vitro. Forskolin increases the amount of intracellular adenosine 3′,5′-cyclic monophosphate, which activates CFTR-mediated fluid secretion.[1] Thus, if CFTR is functional, enteroids will swell in response to forskolin administration.[1,2] Enteroids were imaged before and 1 hour after administration of 5 μM forskolin (Tocris, Bristol, UK) to assess the change in diameter of each individual enteroid in response to adenosine 3′,5′-cyclic monophosphate stimulation. A JuLi stage microscope (NanoEnTek, Seoul, Korea) was used to image the forskolin swelling assay, which was performed at 37°C with 5% CO_2. Enteroid swelling was quantified using Fiji software (formerly known as ImageJ). The forskolin swelling assay data represent 3 independent experiments.

Fecal Chloride Measurement

Pig feces were collected and 0.1 g of feces were resuspended in 500 μL Milli-Q water (Millipore, Billerica, MA). Samples were thoroughly mixed and centrifuged at 5000*g* for 5 minutes at 4°C to pellet intestinal solids. Cl^- concentrations were determined from the resulting supernatant using a microchloride ion electrode (LIS-146CLCM; Lazar, Los Angeles, CA) and normalized to mM per gram feces.

Human Tissue Approval

This study used archival paraffin tissue from the duodenum of healthy individuals and patients with MVID through approved Institutional Review Boards at Phoenix Children's Hospital and Vanderbilt University Medical Center.

Statistics

Values are reported as the mean ± standard error of the mean. Statistical significance for the forskolin swelling assay was determined using a 2-tailed Student *t* test using Prism GraphPad Software (GraphPad, La Jolla, CA). A *P* value $<.05$ was considered significant.

Supplementary References

1. Dekkers JF, Wiegerinck CL, de Jonge HR, et al. A functional CFTR assay using primary cystic fibrosis intestinal organoids. Nat Med 2013;19:939–945.
2. Boj SF, Vonk AM, Statia M, et al. Forskolin-induced swelling in intestinal organoids: an in vitro assay for assessing drug response in cystic fibrosis patients. J Vis Exp 2017 Feb 11:120.
3. Lee MG, Wigley WC, Zeng W, et al. Regulation of Cl-/ HCO3- exchange by cystic fibrosis transmembrane conductance regulator expressed in NIH 3T3 and HEK 293 cells. J Biol Chem 1999;274:3414–3421.
4. Ameen NA, Marino C, Salas PJ. cAMP-dependent exocytosis and vesicle traffic regulate CFTR and fluid transport in rat jejunum in vivo. Am J Physiol Cell Physiol 2003;284:C429–C438.
5. French PJ, van Doorninck JH, Peters RH, et al. A delta F508 mutation in mouse cystic fibrosis transmembrane conductance regulator results in a temperature-sensitive processing defect in vivo. J Clin Invest 1996;98:1304–1312.

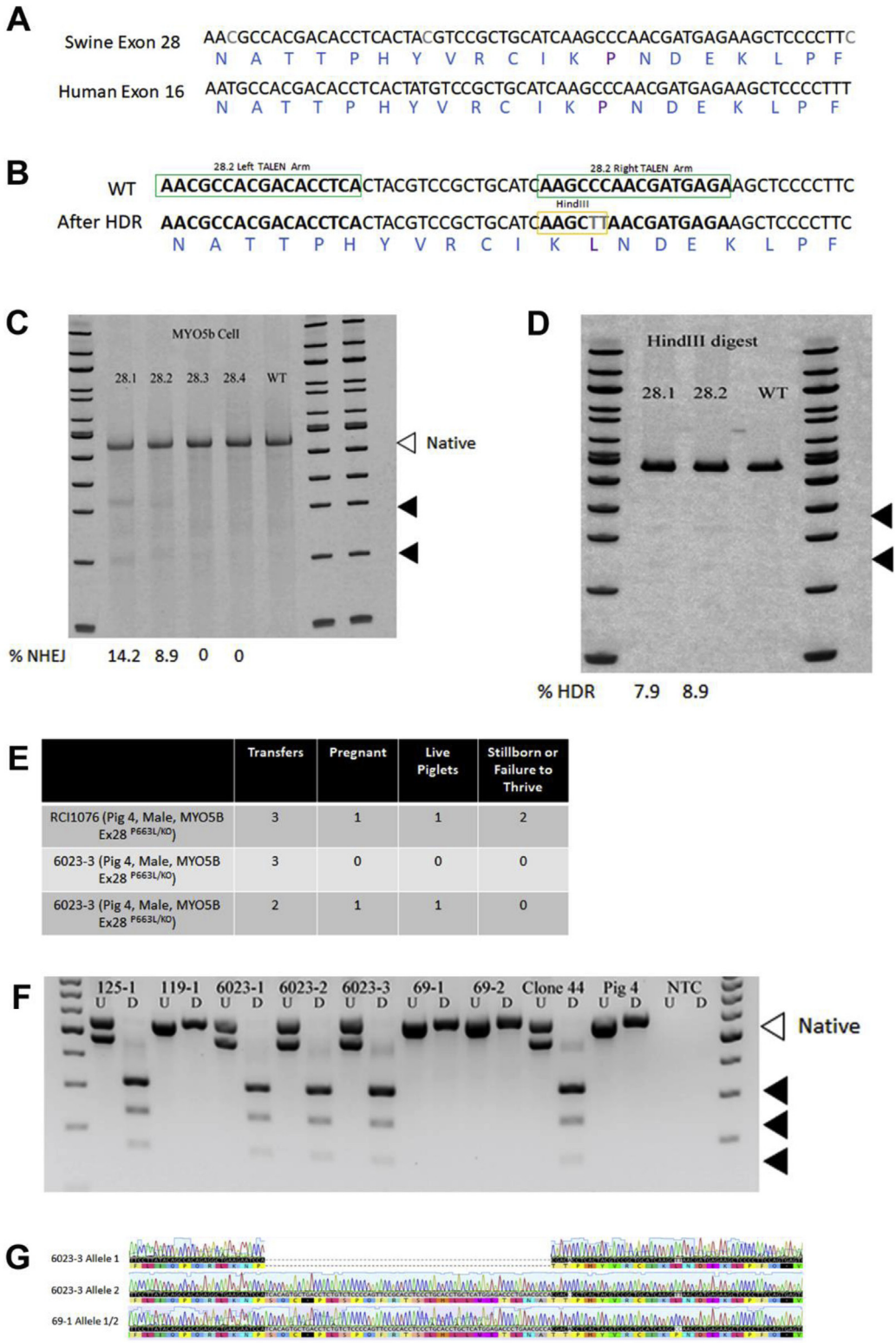

	Transfers	Pregnant	Live Piglets	Stillborn or Failure to Thrive
RCI1076 (Pig 4, Male, MYO5B Ex28 $^{P663L/KO}$)	3	1	1	2
6023-3 (Pig 4, Male, MYO5B Ex28 $^{P663L/KO}$)	3	0	0	0
6023-3 (Pig 4, Male, MYO5B Ex28 $^{P663L/KO}$)	2	1	1	0

Supplementary Figure 1. Development of MYO5B P663L gene–edited Landrace swine model of MVID. (*A*) A portion of exon 28 and exon 16 of swine and human *MYO5B* gene, respectively, shows a nucleotide and protein alignment. This gene is well conserved between both species at an amino acid (AA) level of 83%. The mutation corresponds to a substitution of the AA Proline at position 660 and 663 in humans and swine, respectively. *Gray letters* indicate differences in nucleotide sequence in comparison to human; *blue* indicates AA sequence; *purple letters* indicate Proline 660 or 663. (*B*) The MYO5B^{P663L} homologous recombination (HR) template was designed around the chosen TALEN containing the P663L mutation, a unique HindIII site for RFLP to facilitate screening of HR-positive cells and animals, was introduced due to the intended mutation and provide mutations to eliminate TALEN re-binding to the targeted allele once HR occurred. *Gray letters* indicate differences in nucleotide sequence after HR occurred; *bold letters* indicate TALEN binding site; *purple letter* indicates L663. (*C*) *Gel image* of Surveyor assay on transfected Landrace fetal fibroblast with 1 μg of TALEN messenger RNA (mRNA). Cells were recovered for 3 days at 30°C before quantification. The *open arrowhead* denotes the WT allele and the *closed arrowhead* denotes the RFLP or cut allele. (*D*) *Gel image* of an RFLP assay on male Landrace fetal fibroblast that were transfected with 1 μg of TALEN mRNA and 0.2 nMol of the HR template. These cells were recovered for 3 days at 30°C before quantification. (*E*) *Table* of the selected gene-edited pooled male fetal fibroblast used for somatic cell nuclear transfer and the outcomes. (*F*) *Gel image* of an RFLP assay on the mutant and wild type control animals. (*G*) Sequencing results of a semi-homozygous (MYO5B$^{P663L/KO}$) cloned (6023-3) animal and a WT control animal (69-1).

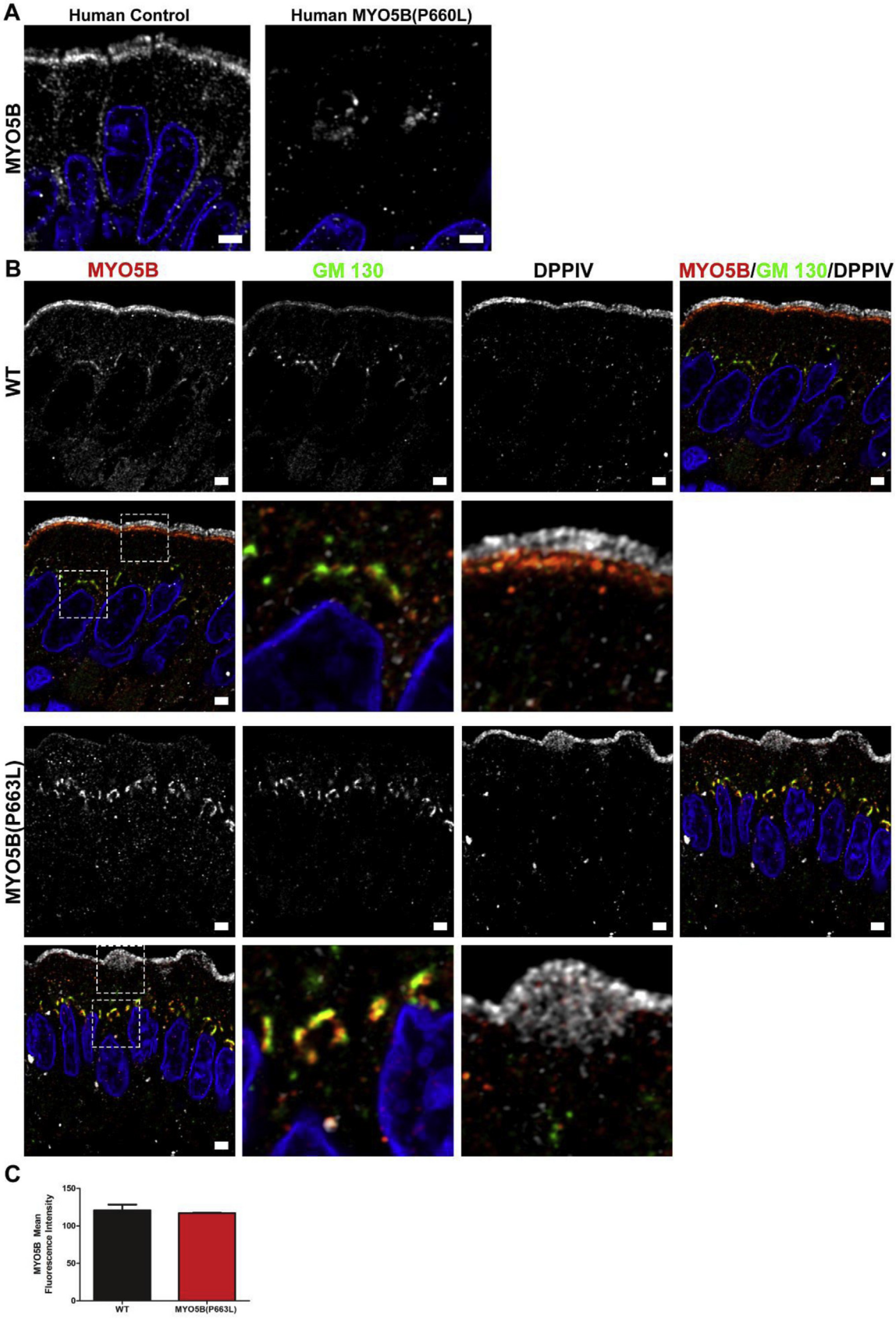
A
Human Control
Human MYO5B(P660L)
MYO5B
B
MYO5B
GM 130
DPPIV
MYO5B/GM 130/DPPIV
WT
MYO5B(P663L)
C
MYO5B Mean Fluorescence Intensity
150
100
50
0
WT
MYO5B(P663L)

Supplementary Figure 2. Expression of MYO5B in humans and pigs with Navajo mutation in MYO5B. (*A*) Immunostaining of biopsies from healthy (control) and MVID duodenum for MYO5B (*white*). Control biopsy demonstrated MYO5B expression primarily at the base of the apical brush border of enterocytes. Human MVID biopsies showed internalized MYO5B that was not closely aligned with the brush border; n = 3 biopsies per group. (*B*) *Immunofluorescence micrograph* showing MYO5B (*red*), the Golgi apparatus marker GM130 (*green*), and the brush border enzyme DPPIV (*white*) in WT and MYO5B(P663L) swine enterocytes. MYO5B was localized to the base of the brush border in WT duodenum while in MYO5B(P663L) duodenum MYO5B was associated with the Golgi apparatus. DPPIV identified the brush border and was observed subapically in MYO5B(P663L) pigs. (*C*) Quantification of mean fluorescence intensity of MYO5B in WT and MYO5B(P663L) pig duodenum. Data reported as mean ± standard error of the mean. Scale bars: 2 μm, n = 2 MYO5B(P663L) pigs and 3 WT pigs.

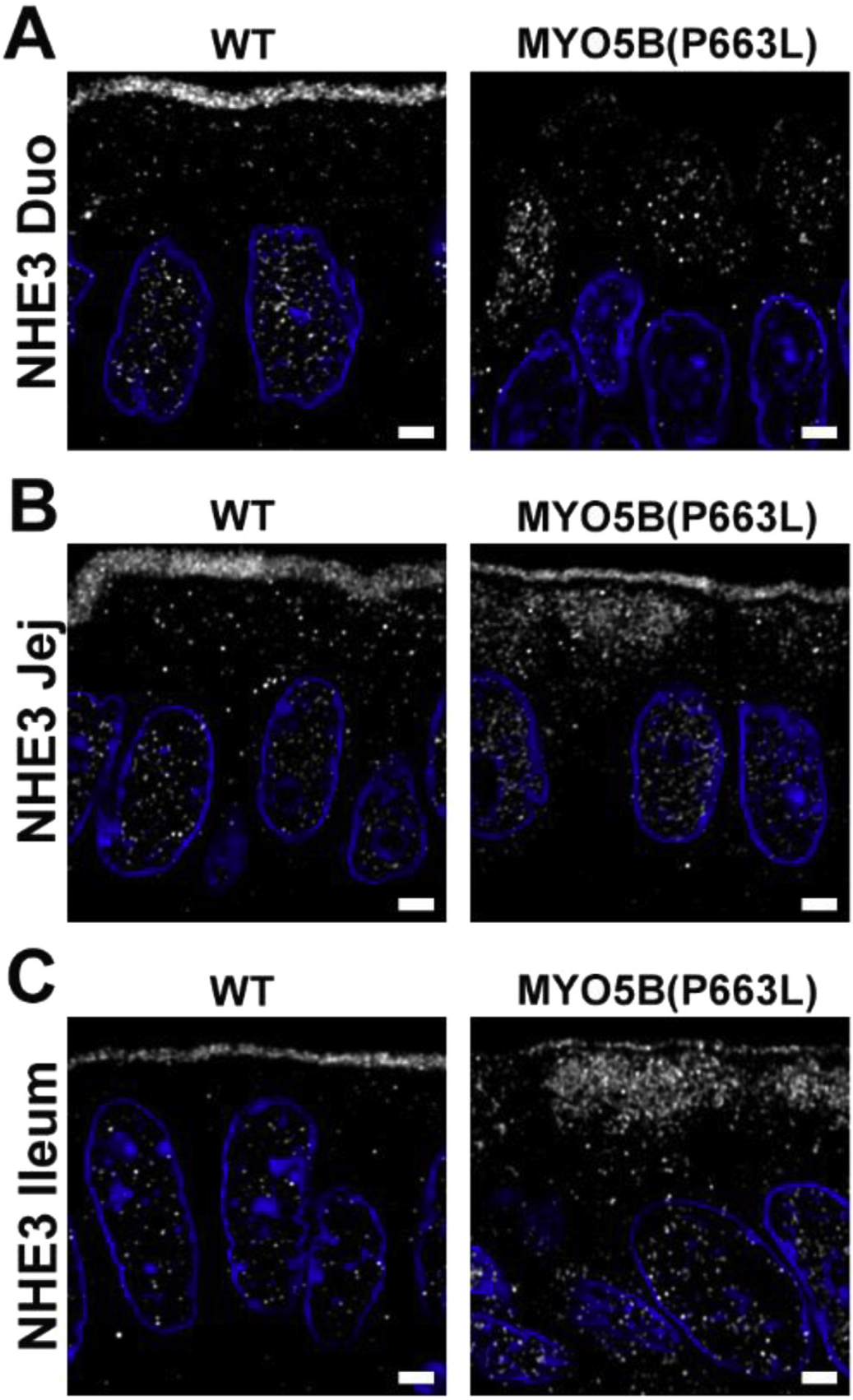

Supplementary Figure 3. NHE3 is mislocalized in the jejunum and ileum of MYO5B(P663L) pigs. *Immunofluorescence images* of NHE3 in WT and MYO5B(P663L) enterocytes along the length of the small intestine. NHE3 was present in the apical membrane of enterocytes in WT pigs. In MYO5B(P663L) NHE3 was mislocalized, similar to the duodenum, in the jejunum and the ileum. Scale bars: 50 μm in low magnification, scale bars: 2 μm in high magnification, n = 2 MYO5B(P663L) pigs and 3 WT pigs.

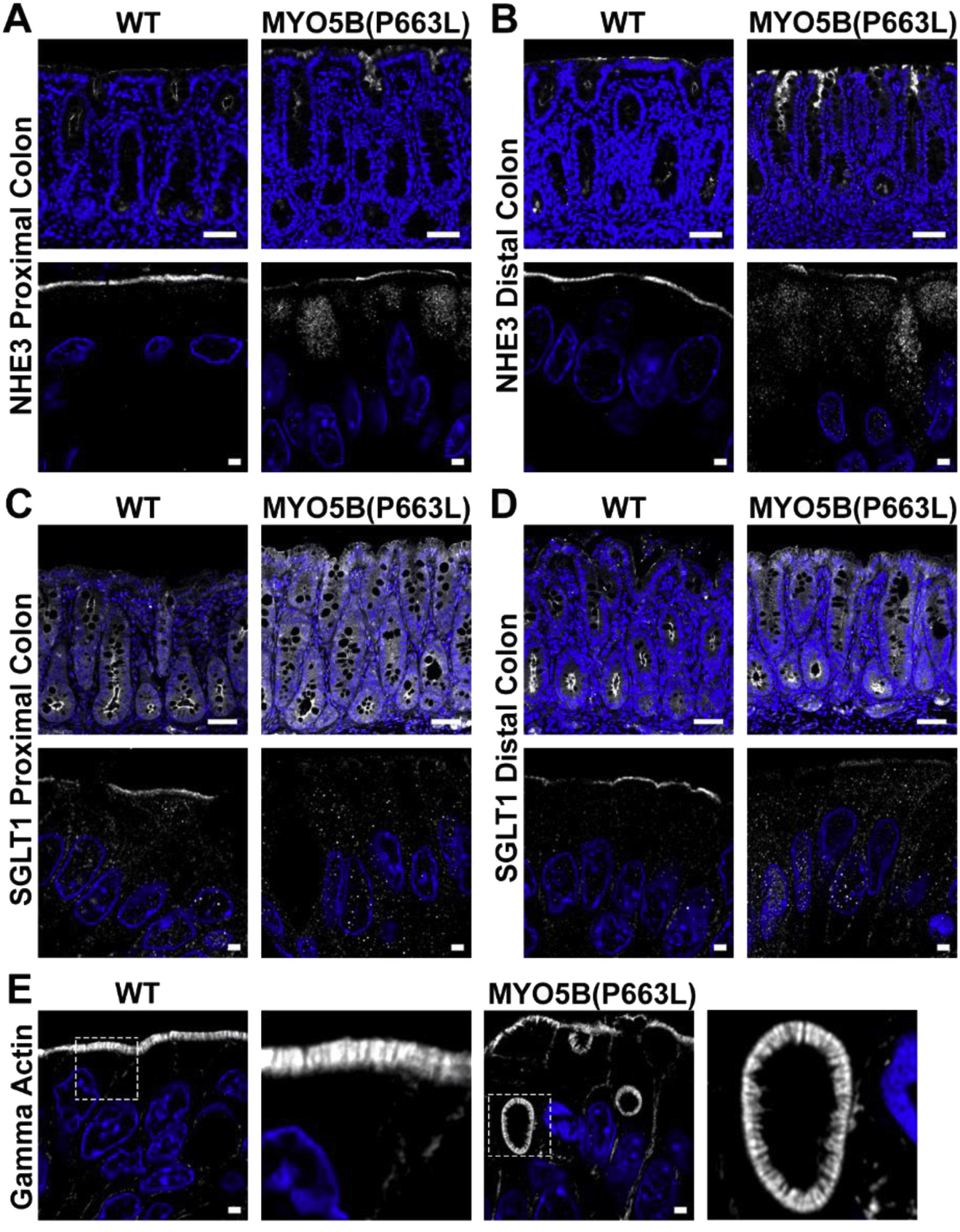
A
WT
MYO5B(P663L)
NHE3 Proximal Colon
B
WT
MYO5B(P663L)
NHE3 Distal Colon
C
WT
MYO5B(P663L)
SGLT1 Proximal Colon
D
WT
MYO5B(P663L)
SGLT1 Distal Colon
E
WT
MYO5B(P663L)
Gamma Actin

Supplementary Table 1. List of Primary Antibodies Used for Immunofluorescence Staining

Antibody	Company	Catalog	Dilution
Alkaline phosphatase	Rockland	200-4135S	1:2000
BSEP	Tamiya Biomedical	PC-064	1:200
CD10	Abcam	Ab951	1:50
CFTR	Gift from Christopher Marino	R3194[3-5]	1:200
DPPIV	R&D Systems	AF1180	1:200
Gamma actin	Santa Cruz Biotech	SC-65638 AF647	1:100
GM130	BD Biosciences	610822	1:200
MDR1	Abcam	Ab3366	1:200
MRP2	Enzo	ALX-801-016-C250	1:200
MYO5B	Novus Biologicals	NBP1-87746	1:200
NHE3	Novus Biologicals	NBP1-82574	1:100
p120	BD Biosciences	610133	1:200
P-ERM	Cell Signaling Tech	3726	1:200
Rab11a	US Biologicals	R009	1:200
SGLT1	Novus Biologicals	NBP 238748	1:100

Supplementary Figure 4. Changes in apical localization of sodium transporters are present in the proximal and distal colon of MYO5B(P663L) pigs. (*A, B*) *Micrographs* of NHE3 immunostaining in the proximal and distal colon of WT and MYO5B(P663L) pigs. MYO5B(P663L) pigs showed subapical localization of NHE3 in the large intestine compared to WT pigs. (*C, D*) Immunostaining of SGLT1 in the proximal and distal colon of WT and MYO5B(P663L) pigs. MYO5B(P663L) pigs had decreased apical SGLT1 compared to WT pigs. (*E*) Gamma actin staining demonstrated the presence of inclusions lined by microvilli in the colon of MYO5B(P663L) pigs. No inclusions were observed in WT pigs. Scale bars: 50 μm in low magnification, scale bars: 2 μm in high magnification.